ÇUKUROVA UNIVERSITY
INSTITUTE OF NATURAL AND APPLIED SCIENCE

MSC THESIS

Tansu DOGAN

FINITE ELEMENT SIMULATION OF THE ELECTROMAGNETIC ABSORPTION IN HUMAN HEAD

DEPARTMENT OF ELECTRICAL AND ELECTRONICS ENGINEERING

ADANA, 2012

ÇUKUROVA UNIVERSITY
INSTITUTE OF NATURAL AND APPLIED SCIENCES

FINITE ELEMENT SIMULATION OF THE ELECTROMAGNETIC ABSORPTION IN HUMAN HEAD

Tansu DOGAN

MSc THESIS

DEPARTMENT OF ELECTRICAL AND ELECTRONICS ENGINEERING

We certify that the thesis titled above was reviewed and approved for the award of degree of the Master of Science by the board of jury on 03/09/2012.

…….....	……...	…….....
Asst. Prof. Dr. M.Kerem UN	Prof. Dr. Turgut İKİZ	Asst. Prof. Dr. C.Veysel BAYSAL
SUPERVISOR	MEMBER	MEMBER

This MSc Thesis is written at the Department of Institute of Natural And Applied Sciences of Çukurova University.
Registration Number:

Prof. Dr. Selahattin SERİN
Director
Institute of Natural and Applied Sciences

Not: The usage of the presented specific declerations, tables, figures, and photographs either in this thesis or in any other reference without citiation is subject to "The law of Arts and Intellectual Products" number of 5846 of Turkish Republic

ABSTRACT

MSc THESIS

FINITE ELEMENT SIMULATION OF THE ELECTROMAGNETIC ABSORPTION IN HUMAN HEAD

Tansu DOGAN

ÇUKUROVA UNIVERSITY
INSTITUTE OF NATURAL AND APPLIED SCIENCES
DEPARTMENT OF ELECTRICAL AND ELECTRONICS ENGINEERING

Supervisor : Asst. Prof. Dr. M. Kerem ÜN
Year: 2012, Page: 65
Jury : Asst. Prof. Dr. M. Kerem ÜN
: Prof. Dr. Turgut İKİZ
: Asst. Prof. Dr. C. Veysel BAYSAL

Potential health risks associated with the usage of cellular phones is a debated issue. The electromagnetic waves in the radio frequency band, emitted by the cellular phone, are absorbed by the bodily tissues, particularly those in the head, resulting to heating. Standards have been set for the allowed amount of exposure in terms of specific absorption rate (SAR), which is the energy absorbed by a unit mass of tissue per unit time. The absorption rate depends on the geometry, properties and relative location of the source as well as the geometry and the electromagnetic properties of the absorbing tissue. While it is possible to determine the absorption level through experimentation, numerical simulation offers a convenient way of estimating it for actual or hypothetical configurations. While finite difference time domain (FDTD) method is the most widely used approach in the numerical simulation of such phenomena, finite element method (FEM) studies are relatively rare. The objective of this work is to establish a FEM environment to simulate the electromagnetic absorption and the resulting temperature rise associated with the tissues in the head due to cellular phone usage. The analyses have been performed using COMSOL package. The SAR value has been found to exceed the set standards if the phone transmits with a relatively high power. The resulting temperature rise has been typically small but its long term health effects are a matter of further research.

Keywords: Electromagnetic Absorption, A FEM Application, Health Risks of Mobile Phones

ÖZ

YÜKSEK LİSANS TEZİ

İNSAN KAFASINDAKİ ELEKTROMANYETİK SOĞURULMANIN SONLU ELEMANLAR SİMULASYONU

Tansu DOGAN

ÇUKUROVA ÜNİVERSİTESİ
FEN BİLİMLERİ ENSTİTÜSÜ
ELEKTRİK ELEKTRONİK MÜHENDİSLİĞİ ANABİLİM DALI

Danışman : Yrd. Doç. Dr. M. Kerem ÜN
Yıl: 2012, Sayfa: 65
Jüri : Yrd. Doç. Dr. M. Kerem ÜN
: Prof. Dr. Turgut İKİZ
: Yrd. Doç. Dr. C. Veysel BAYSAL

Cep telefonu kullanımının sağlık riskleri yaratabileceği tartışılan bir konudur. Telefonlar tarafından saçılan radyo frekansı bandındaki elektromanyetik dalgalar, vücut dokuları, özellikle kafadaki dokular tarafından soğrularak ısınmaya yol açmaktadır. Maruz kalınan miktara yönelik olarak Özgül Soğurulma Hızı (SAR) (Birim zamanda birim kütle tarafından emilen enerji miktarı) cinsinden standartlar belirlenmiştir. Soğurulma hızı, kaynağın geometrisi, özelliği ve göreli konumuna bağlı olduğu kadar, soğuran dokunan geometrisi ve elektromanyetik özellikleriyle de ilgilidir. Soğurulma hızını deneysel olarak belirlemek olası ise de sayısal benzetim bu hızı gerçek ve hayali durumlarda tahmin etmek için olası bir yol oluşturur. Bu tür olguların sayısal benzetiminde sonlu farklar (FDTD) yöntemi en sık kullanılan sayısal yaklaşımken, sonlu elemanlar yönteminden (FEM) yararlanılan çalışmalar az sayıdadır. Bu tezin amacı, cep telefonu kullanımı yüzünden kafadaki dokularda gerçekleşen elektromanyetik soğurulmayı ve buna bağlı olan sıcaklık yükselmesini simüle etmek üzere bir sonlu elemanlar ortamı oluşturmaktır. Analizler COMSOL paket programı kullanılarak yapılmıştır. Telefon nispeten yüksek güç kullandığında, SAR değerinin belirlenen standartların üstünde olduğu görülmüştür. Elde edilen sıcaklık artışı genelde küçüktür fakat uzun vadeli sağlık etkileri daha ileri çalışmalar için bir konu teşkil etmektedir.

Anahtar kelimeler: Elektromanyetik Soğurulma, Bir FEM Uygulaması, Cep Telefonlarının Sağlık Riskleri

ACKNOWLEDGEMENTS

I would like to express my heartfelt gratitude to my advisor Asst. Prof. Dr. M. Kerem ÜN for his supervision, guidance, encouragement, and extremely useful suggestions throughout this thesis study. It has been a great honor to work with him. I would also like to thank my committee members, Prof. Dr. Turgut İKİZ and Asst. Prof. Dr. Cabbar Veysel BAYSAL for evaluating my thesis and providing me with important feedback.

I would like to thank Mr. Ahmet ÇALIK for his valuable advice and technical support in finite element related issues.

I wish to extend my acknowledgements to all staff members in the Electrical-Electronics Engineering Department and my friends.

Last but not the least, I would like to thank my family for their endless support and encouragement throughout this study.

CONTENTS **PAGE**

ABSTRACT I
ÖZ II
ACKNOWLEDGEMENTS III
CONTENTS IV
LIST OF TABLES VI
LIST OF FIGURES VII
SYMBOLS AND ABBREVIATONS XI
l. INTRODUCTION 1
1.1. Background 1
1.2. Effect of Electromagnetic Waves on Life Tissue 2
1.3. Numeric Modeling of Electromagnetic Wave Propagation in Tissues 3
1.4. The Scope of This Thesis 6
2. ELECTROMAGNETIC WAVES, BIOHEAT TRANSFER 3
2.1. Maxwell Equations 7
2.2. Helmholtz Equations 10
2.3. Bioheat Transfer Equation 16
2.4. Coupling of the Equations, Specific Absorption Rate (SAR) 17
3. FINITE ELEMENT METHOD (FEM) FOR ELECTROMAGNETICS 19
3.1. Method of Weighted Residual 20
3.2. Boundary and Interface Conditions 21
3.3. Perfectly Matched Layers (PMLs) in the Models 22
4. GEOMETRIC MODELS 25
4.1. Introduction 25
4.2. The Homogeneous Head Model 25
4.3. The Nonhomogeneous Head Model 29
4.4. Patch Antenna Model 33
5. NUMERIC SIMULATION 35
5.1. Problem Parameters 35
5.2. Finite Element Mesh 38

5.3. The Analysis 41
5.4. The Results of Homogeneous Model.....42
5.5. The Results of Nonhomogeneous Model.....45
6. DISCUSSION AND CONCLUSION.....55
REFERENCES.....59
CURRICULUM VITAE 64

LIST OF TABLES **PAGE**

Table 4.1. The Dimensions of Homogeneous Head Model 27
Table 4.2. The Antenna Dimensions Used in This Study 34
Table 5.1. Problem Parameters in Used Program for Homogeneous Study at 900 MHz 35
Table 5.2. Problem Parameters in Used Program for Homogeneous Study at 1800 MHz 36
Table 5.3. Problem Parameters in Used Program for Nonhomogeneous Study at 900 MHz 36
Table 5.4. Problem Parameters in Used Program for Nonhomogeneous Study at 1800 MHz 37
Table 5.5. The Conditions of Studies 41
Table 5.6. The Parameter of Metabolic Heat Source 42
Table 5.7. The Calculated the Electric Field, SAR and Temperature Rise For Homogeneous and Nonhomogeneous Head Models 55
Table 5.8. A Comparison with Nonhomogeneous FEM and FDTD Head Models 57

LIST OF FIGURES **PAGE**

Figure 1. Cross section of central brain of (A) unexposed control rat and (B) RF frequency exposed rat 2
Figure 2. Number of scientific papers on the finite element method published yearly from 1969 to 1992.....4
Figure 3. In terms of EM spectrum, cell phones fall between the microwaves owen and TV transmitters or FM radios 7
Figure 4. Schematic representation of electromagnetic field 9
Figure 5. Basic Finite Elements: 1-D: Line element, 2-D: Triangle, Quadrilateral and 3-D: tetrahedron, pentahedron and hexahedron 19
Figure 6. An example picture of finite PML in the problem space surface model 23
Figure 7. An example of MRI pictures used in homogeneous head model 26
Figure 8. The homogeneous FEM head and patch antenna model in realistic dimensions.....26
Figure 9. The numeric FEM head and patch antenna model in realistic dimensions 27
Figure 10. The view of problem space along the z axis.....28
Figure 11. The view of problem space along the x axis.....28
Figure 12. The view of problem space along the y axis.....29
Figure 13. The size of MRI data used in FEM nonhomogeneous head Model (xz direction).....30
Figure 14. The size of MRI data used in FEM nonhomogeneous head Model (xy direction) 31
Figure 15. The size of MRI data used in FEM nonhomogeneous head Model (yz direction).....31
Figure 16. The views of head model's layers (A) The skin and fat tissues are coupled. (B) The skull layer. (C) The skull, skin and fat tissues are coupled. (D) The brain layer.....32

Figure 17. The head model with layers indicated 32
Figure 18. The general view of the problem space (Air, head model and patch antenna).....33
Figure 19. The finite element mesh for homogeneous head, patch antenna and air.....38
Figure 20. The picture of homogeneous head mesh space.....39
Figure 21. Another picture of head mesh space.....39
Figure 22. The finite element mesh of the head 40
Figure 23. Another picture of realistic model's finite element mesh space.....40
Figure 24. The log (SAR) values at 900 MHz and 0.25 W antenna power has a maximum 0.711 W/kg SAR value in homogeneous model.....43
Figure 25. The local increase in surface temperature at 900 MHz and 0.25 W antenna power has a maximum 37.487 ºC right beneath the antenna in homogeneous model.....43
Figure 26. The isosurface temperature contours at 900 MHz and 0.25 W antenna power in homogeneous model.....44
Figure 27. The log (SAR) values at 1800 MHz and 0.25 W antenna power has a maximum 0.906 W/kg SAR value in homogeneous model.....44
Figure 28. The EM field propagation at 900 MHz and 0.25 W antenna power has a maximum 81.440 V/m value in nonhomogeneous model.....46
Figure 29. The local increase in surface temperature at 900 MHz and 0.25 W antenna power with thermal insulation boundary conditions has a maximum 37.276 ºC right beneath the antenna in nonhomogeneous model.....46
Figure 30. The contour temperature lines at 900 MHz and 0.25 W antenna power with thermal insulation boundary conditions in nonhomogeneous model 47
Figure 31. The local increase in surface temperature at 900 MHz and 0.25 W antenna power with convective cooling boundary conditions has

a maximum 37.270 ºC right beneath the antenna in nonhomogeneous model.....47
Figure 32. The contour temperature lines at 900 MHz and 0.25 W antenna power with convective cooling boundary conditions in nonhomogeneous model 48
Figure 33. The EM field propagation at 1800 MHz and 0.25 W antenna power has a maximum 80.453 V/m value in nonhomogeneous model 48
Figure 34. The local increase in surface temperature at 1800 MHz and 0.25 W antenna power with convective cooling boundary conditions has a maximum 37.207 ºC right beneath the antenna in nonhomogeneous model 49
Figure 35. The contour temperature lines at 1800 MHz and 0.25 W antenna power with convective cooling boundary conditions in nonhomogeneous model 49
Figure 36. The EM field propagation at 900 MHz and 1 W antenna power has a maximum 162.88 V/m value in nonhomogeneous model.....50
Figure 37. The local increase in surface temperature at 900 MHz and 1 W antenna power with convective cooling boundary conditions has a maximum 37.646 ºC right beneath the antenna in nonhomogeneous model 50
Figure 38. The contour temperature lines at 900 MHz and 1 W antenna power with convective cooling boundary conditions in nonhomogeneous model 51
Figure 39. The EM field propagation at 1800 MHz and 1 W antenna power has a maximum 160.93 V/m value in nonhomogeneous model 51
Figure 40. The local increase in surface temperature at 1800 MHz and 1 W antenna power with convective cooling boundary conditions has a maximum 37.378 ºC right beneath the antenna

in nonhomogeneous model 52
Figure 41. The contour temperature lines at 1800 MHz and 1 W antenna power with convective cooling boundary conditions in nonhomogeneous model 52
Figure 42. The local increase in surface temperature at 900 MHz and 1 W antenna power with metabolic heat source and convective cooling boundary conditions has a maximum 37.652 ºC right beneath the antenna in nonhomogeneous model.....53
Figure 43. The isothermal contour temperature lines at 900 MHz and 1 W antenna power with metabolic heat source and convective cooling boundary conditions in nonhomogeneous model.....53

SYMBOLS AND ABBREVIATIONS

Q_{met} : Metabolic Heat Source

E : Electric Field Intensity

D : Electric Flux Density

B : Magnetic Flux Density

H : Magnetic field intensity

J : Electric current density

μ_r : Relative Permeability of the material

μ_0 : Permeability of vacuum

ρ : Electric charge density

σ_r : Electrical conductivity tensor

ε_r : Relative permittivity of the material

ε_0 : Permittivity in vacuum

λ : Wavelength

f : Frequency

k : Thermal conductivity

C : Heat capacity at constant pressure

rho : Density of tissue

ρ_b : Density of blood

C_b : Specific heat of blood

w_b : Blood perfusion rate

T_b : Arterial blood temperature

T_{ext} : External temperature

h : Heat transfer coefficient

k_0 : Free space wave number

ω : Angular frequency

β : Propagation constant

W	:	Energy density
A	:	Magnetic potential (vector)
d	:	Penetration depth
q_r	:	Radiative heat flux
T_{inf}	:	Temperature of the external fluid
FEM	:	Finite Element Method
FDTD	:	Finite Difference Time Domain
SAR	:	Specific Absorption Rate
EM	:	Electromagnetic
RF	:	Radio Frequency
MM	:	Methods of Moment
TDMA	:	Time Division Multiple Access
GSM	:	Global System of Mobile Communications
EMF	:	Electromagnetic Field
DCS	:	Digital Cellular Service
Hz	:	Hertz
FM	:	Frequency Modulation
PMLs	:	Perfect Match Layers
MRI	:	Magnetic Resonance Imaging
IEEE	:	The Institute of Electric and Electronics Engineer
b.c.	:	Boundary Conditions
ICNIRP	:	International Commission for Non-Ionizing Radiation Protection
WHO	:	World Health Organization

1. INTRODUCTION

1.1. Background

The radio waves have been used in a hundred years and their usage is increasing day by day. Today, radio waves play a role in communication systems, remote control, medical diagnosis and treatment devices, environmental training, marketing and military systems. Despite their widespread usage, their effect on human health is not well understood.

In late 1800s, the French scientists, d'Arsonval, investigated the physiological effects of the radio waves and made some researchs on the effects of heat on the human health. Arsonval reported on a flickering visual sensation perceived when an individual's head was placed within a strong time–varying magnetic field. This was the first experiment on magnetic stimulation of the nervous system.

Developments of the radar and medical applications have helped to understand the interaction between human tissue and radar. Invented some 60 years ago, radar systems have been widely used for navigation, aviation, national defense and weather forecasting. Their primary objectives are individual and collective safety and protection. People who live or routinely work around radars have expressed concerns about long-term adverse effects of these systems on health, including cancer, reproductive malfunction, cataracts and changes in behavior or development of children (E. Knot et al, 1985).

The effect of electromagnetic waves on human health is still a matter of debate and research. Numerical simulation of electromagnetic wave absorption and the related heating in the tissue can be an important tool to assist the research efforts in this issue which is the topic of the current work. In this study, we have used the finite element method (FEM) to simulate the electromagnetic wave absorption due to cellular phone usage and the resulting temperature increase in the human head, consist of skin-fat, bone and brain tissues.

1.2. Effect of Electromagnetic Waves on Life Tissue

Research indicates that partial or whole exposure of human and animal body to RF radiation (as due to mobile phone usage) may lead to a variety of changes in tissues (Behari J, 2010). The radiation from TDMA digital cellular phones can cause significant changes in ornithine decarboxylase activity (ODC), which is essential for DNA synthesis. (Penafiel et al, 1997). In other studies, increases in DNA breaks are observed at 2.45 and 50 GHz. (Sarkar et al, 1984; Lai and Sing et al, 2004). On the other hand, 24 hours of exposure to 935 MHz basic signal at 1 or 2 W/kg SAR values is shown not to cause any DNA strand breaks in human blood cells (Stronati et al, 2006). In another related study, four hours of GSM–900 MHz exposure of the brain at a power density ranging of 7.5 W/kg has resulted to a significant increase in albumin extravasation due to the thermal effect of the electromagnetic wave (Nittby et al, 2009) which can cause cellular dehydration.

Salford et al have studied the effects of microwave exposure from the GSM mobile phones on nerve cells Fischer 344 rats are divided into four groups where the groups are subject to varying levels of electromagnetic radiation. The subject in the control group, with one exception, shows no positivity albumin outside the hypothalamus. In the subjects of the other groups, the albumin has spread in the tissue between the cell bodies and surrounding neurons (Figure 1).

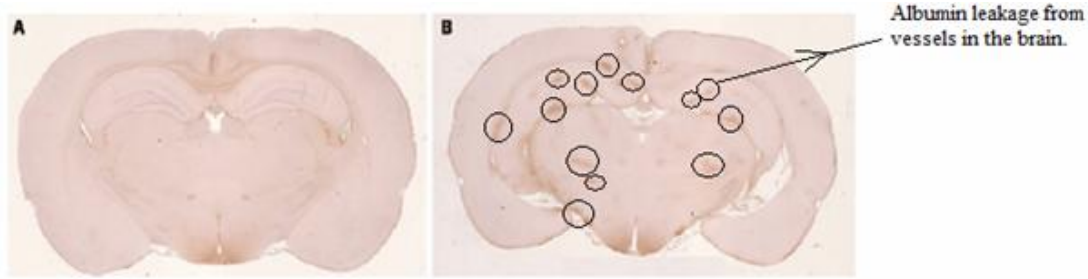


Figure 1. Cross section of central brain of (A) unexposed control rat and (B) RF frequency exposed rat. The (A) albumin is visible in the central inferior parts of the brain (hypothalamus), which is a normal feature but in the (B), albumin is visible in multiple small darkening which are leakage from vessels.

The rapid development of the telecommunication sector in the last decade raises health concerns in the public. These concerns are not totally unsubstantiated because studies reveal that the absorption of high dozed RF radiation gives rise to heating of the human body tissues which may have some negative effects on the human health.

1.3. Numeric Modeling of Electromagnetic Wave Propagation in Tissues

The electromagnetic wave propagation phenomenon is governed by the well-known Maxwell equations with appropriate assumptions, Maxwell equations could be reduced to the Helmholtz equation which is solved numerically in this work. The details are described in Chapter 2. Analytical solutions for the scalar Helmholtz equation in spherical and spheroidal coordinates, obtained by using the method of separation of variables, exist (Abramovitz et al 1964, Ling, 1987, Nag et al, 1995). These solutions are valid on canonical problem geometries where the problem domain is a sphere or an ellipsoid. For more complex problem geometries, we rely on numerical methods.

Different numerical methods have been proposed for the solution of Helmholtz and classical wave equations. The most popular one of these is the so-called the *Finite Difference Time Domain (FDTD)* method, proposed by Yee (Yee, 1966) and the later simplified by Taflove (Taflove et al, 1975). FDTD is used commonly for simulation in electronics, and machinery. In several studies, FDTD has been applied to analyze the propagation of electric and magnetic fields in various organs/tissues, some of which are described below. In one study, (Sullivan et al, 1988) the specific absorption rate (SAR) is calculated by FDTD method, using incident frequencies 100 and 350 MHz for three different cases: A homogeneous human body in free space, an inhomogeneous human body in free space and an inhomogeneous human body standing on the ground. In another work, numerical simulation of induced electric fields and the specific absorption rate (SAR) produced by microwave radiation from a half wave-length dipole near the tissue is reported. The electromagnetic calculations are done for half – wave dipoles

radiating at 900 and 1900 MHz frequencies and from various distances to the model using the FDTD method. The calculated SAR values are compared with the other analytical studies (Riu at al, 1999).

Another numerical approach to solve the partial differential equations is the finite-element method (FEM) first outlined in 1943 by Courant (Courant, 1943). This method is widely used in mechanical and civil engineering problems, and its usage in electrical engineering problems has been comparatively infrequent. On the other hand, its popularity is on the rise in recent years. The number of articles about finite elements applications in electronic engineering amounted to a small handful in 1969. By 1992, this number increased approximately to 600 new articles published per year. (R. Cocciolil et al, 1996). In the IEEE database, there are 7000 papers whose titles include the phrase “FEM”, while this number is 30000 if the abstracts are searched for the same phrase.

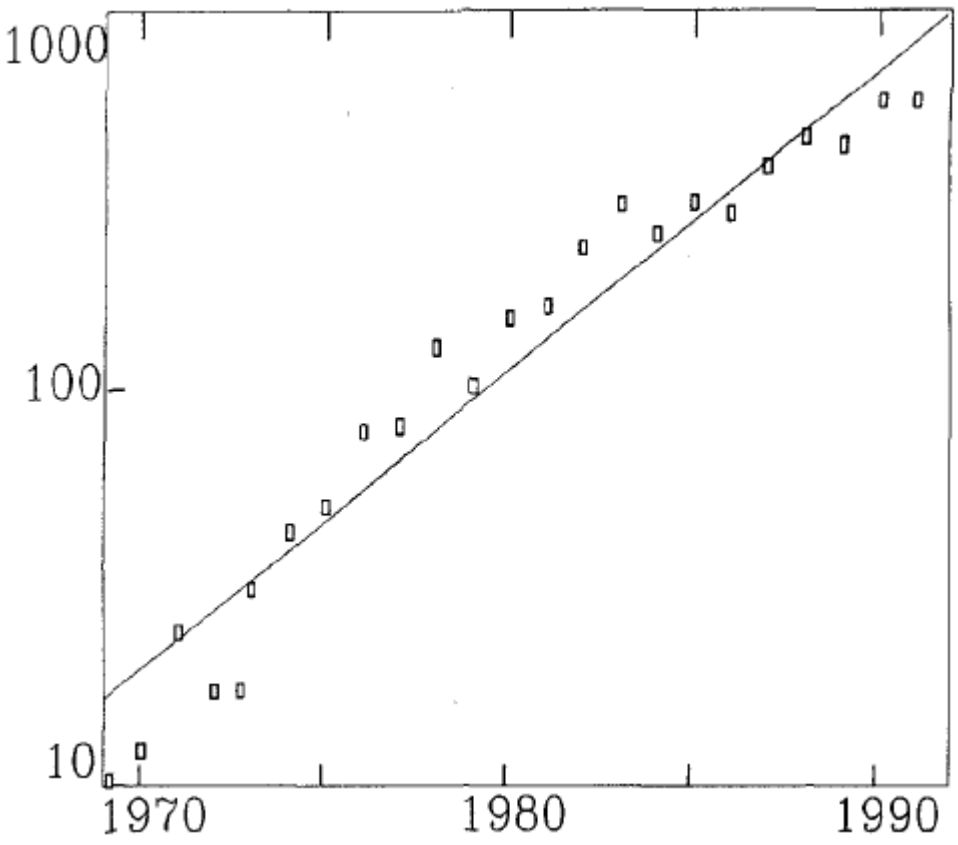


Figure 2. Number of scientific papers on the finite-element method published yearly from 1969 to 1992.

FEM has not been as frequently used to analyze the interaction between EM waves and human body as FDTD. Using the first type of linear vectorial expansion function, FEM analysis performed on an inhomogeneous medium is due Mur (Mur, 1985) which has been followed by numerous other FEM studies analyzing inhomogeneous medium with various configurations using different modifications of the FEM. Few studies are summarized here as follows:

In 1986, Arthur W. Guy studied the quantification of the SAR in human models exposed to UHF mobile antenna fields using thermograph, nonperturbing temperature probes and E-field sensitive divots. The exposure conditions included man, woman, and child models in different positions. In this study, full-scale phantom models, which were filled with synthetic gel having the same dielectric properties as human muscles, were used. In another study, the specific absorption rate (SAR) of electromagnetic radiation from mobile phones on the human head was investigated with using FEM. (S. S. Seker et al, 2002). The human head and the antenna radiated in 900 MHz were simulated in this study. The spherical model as single layer and three layers was simulated by using Agilent High Frequency Structure Simulator, which employs the Finite Element Method (FEM), and the EM power absorption rate of tissue was calculated by a C++ program. The results were compared with the results of the studies in the literature and a good agreement was obtained.

Recently, the temperature increase in the human tissues subjected to electromagnetic waves has been investigated numerically (Wessapan et al, 2011). A 2D finite element model is used to obtain the SAR and temperature increase in human body exposed to electromagnetic wave with different testing condition.

A numerical analysis of specific absorption rate (SAR) and temperature distributions in the realistic human head model exposed to mobile phone radiation at 900 MHz and 1800 MHz are presented by Wessapan (Wessapan, et al, 2012). In the realistic human head model given in this paper, the effects of operating frequency and gap distance between the mobile phone and the human head on distributions of specific absorption rate and temperature profile within the human head are systematically investigated.

1.4. The Scope of This Thesis

In this study, the EM wave propagation, its penetration depth in human tissues and the related temperature rise will be researched using FEM under different conditions.

The definition of the EM waves, their propagation principles, governing equations and bioheat transfer equation with coupling the SAR term will be discussed in Chapter 2. Chapter 3 starts with a brief introduction to the FEM and the related method of weighted residual, boundary and interface conditions and Perfectly Matched Layers (PMLs). The formation of a realistic head model from MRI data to be used in the FEM analysis is included in Chapter 4. The results are presented and analyzed in Chapter 5. Concluding remarks are given in Chapter 6.

2. ELECTROMAGNETIC WAVES, BIOHEAT TRANSFER

2.1. Maxwell Equations

The *electromagnetic wave* (EM) is defined as coupled electrical and magnetical fields propagating simultaneously in space. The propagation velocity of the EM wave is equal to the *speed of light* c. The distance between two consecutive peaks of the wave is defined as the *wavelength* λ. The relationship between light and its wavelength can be expressed as:

$$c = l \cdot f \tag{2.1}$$

where f is the frequency of the wave. The categorization of EM waves according to their frequencies is illustrated in Figure 3.

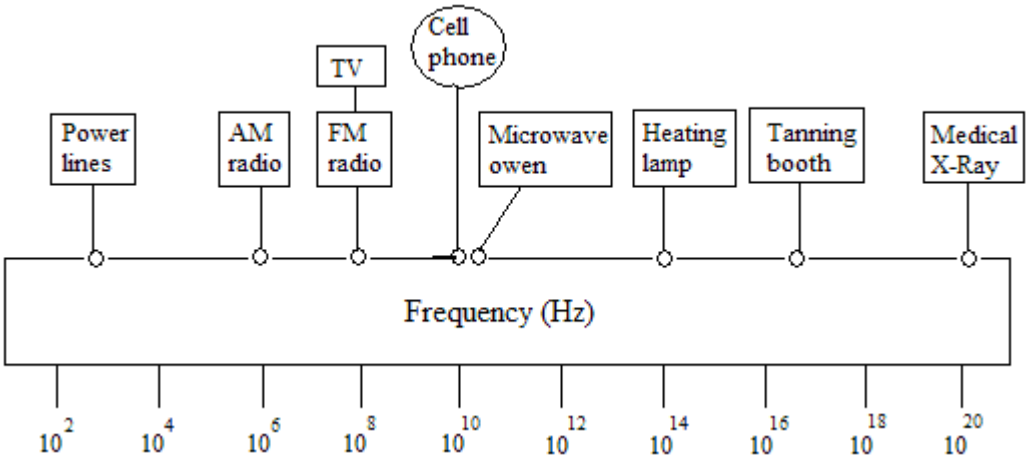


Figure 3. In terms of EM spectrum, cell phones fall between the microwave owen and TV transmitters or FM radios.

The GSM frequency bands used by mobile phone operators in Turkey are 900 MHz and 1800 MHz. which are in microwave frequency band. The microwave band involves EM waves with frequency range 300 MHz – 300 GHz and wavelengths between 1 mm and 1 m.

The EM waves, which are a consequence of accelerated electrical charges, are governed by Maxwell equations:

Electric Gauss' Law $$\nabla \cdot \mathbf{E} = r / e \tag{2.2}$$

Magnetic Gauss' Law $$\nabla \cdot \mathbf{B} = 0 \tag{2.3}$$

Faraday's Law $$\nabla \times \mathbf{E} = -\frac{\partial \mathbf{B}}{\partial t} \tag{2.4}$$

Ampere's Law $$\nabla \times \mathbf{B} = m_0 e_0 \frac{\partial \mathbf{E}}{\partial t} \tag{2.5}$$

The first equation, the electric Gauss' Law, indicates that the electric field flux is conserved at a point unless a nonzero electrical charge density exists at that point. Similarly, the second equation, the magnetic Gauss' Law, points out that the flux of the magnetic field is conserved at every point. According to the third equation, Faraday's Law, a changing magnetic field induces an electrical field. The fourth equation, the Ampere's law, implies that a current or a changing electrical field creates a magnetical field.

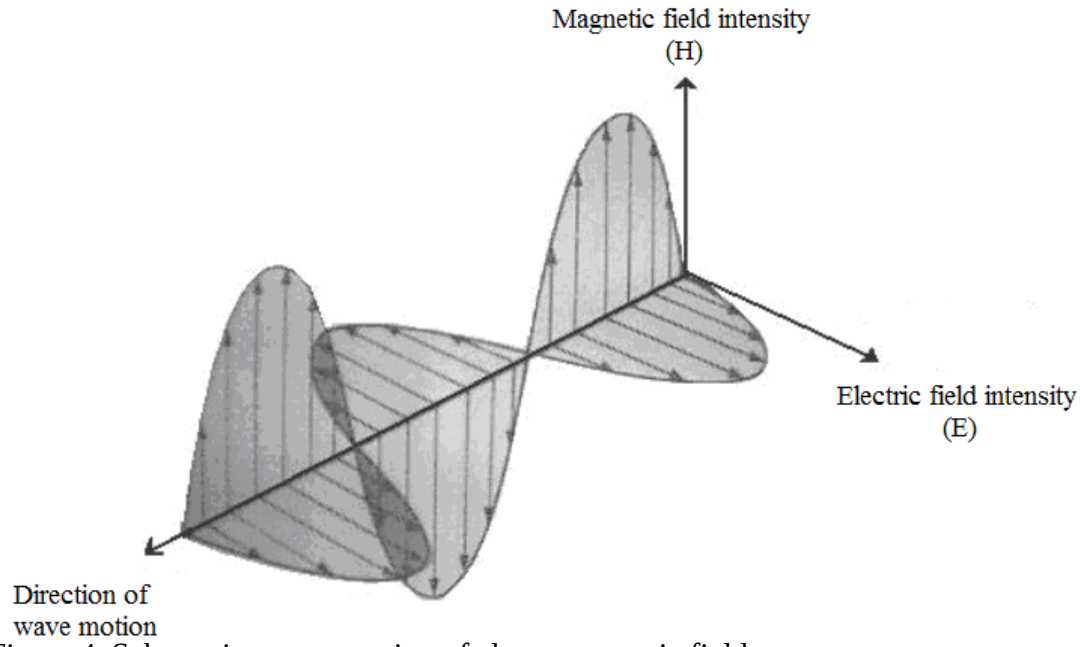


Figure 4. Schematic representation of electromagnetic field.

In free space, we assume that $\rho = 0$, and $\mathbf{J} = \mathbf{0}$ but in the conductive media such as metals or brine these quantities take nonzero values. According to the Ohm law, in the conductive media, free current density (**J**), is proportional to electrical field.

$$\mathbf{J} = s\,\mathbf{E} \tag{2.6}$$

Thus, for a linear conductive media, Maxwell equations take the following form:

$$\nabla \cdot \mathbf{E} = \frac{r}{e} \tag{2.7}$$

$$\nabla \cdot \mathbf{B} = 0 \tag{2.8}$$

$$\nabla \times \mathbf{E} = -\frac{\partial \mathbf{B}}{\partial t} \tag{2.9}$$

$$\nabla \times \mathbf{B} = me \frac{\partial \mathbf{E}}{\partial t} + ms\ \mathbf{E} \tag{2.10}$$

2.2. Helmholtz Equations

The homogeneous Helmholtz equation is obtained from Maxwell equations for free space. As the first step, Eq. 2.4 and 2.5 need to be decoupled. To do that, let us take the curl of the Eq. 2.4:

$$\nabla \times (\nabla \times \mathbf{E}) = -\nabla \times \frac{\partial \mathbf{B}}{\partial t} \tag{2.11}$$

$$\nabla \times (\nabla \times \mathbf{E}) = -\frac{\partial (\nabla \times \mathbf{B})}{\partial t} \tag{2.12}$$

$$\nabla \times (\nabla \times \mathbf{E}) = -\frac{\partial}{\partial t}\left(m_0 e_0 \frac{\partial \mathbf{E}}{\partial t} \right) \tag{2.13}$$

$$\nabla \times (\nabla \times \mathbf{E}) = -m_0 e_0 \frac{\partial^2 \mathbf{E}}{\partial t^2} \tag{2.14}$$

Using a well-known identity:

$$\nabla \times (\nabla \times \mathbf{E}) = \nabla (\nabla \cdot \mathbf{E}) - \nabla \cdot \nabla \mathbf{E} \tag{2.15}$$

But from Eq. 2.2:

$$\nabla \times (\nabla \times \mathbf{E}) = -\nabla \cdot \nabla \mathbf{E} \tag{2.16}$$

Eq. 2.14 becomes

$$\nabla^2 \mathbf{E} = m_0 e_0 \frac{\partial^2 \mathbf{E}}{\partial t^2} \tag{2.17}$$

A similar derivation leads to an identical equation for **B**:

$$\nabla^2 \mathbf{B} = m_0 e_0 \frac{\partial^2 \mathbf{B}}{\partial t^2} \tag{2.18}$$

Therefore, the components of **E** and **B** satisfy the following scalar equation:

$$\nabla^2 f = 1/v^2 \cdot \frac{\partial^2 f}{\partial t^2} \tag{2.19}$$

This is known as *classical wave equation* in free space and describes the wave propagation with light velocity v, where the value of v is given by:

$$v = \frac{1}{\sqrt{m_0 e_0}} \tag{2.20}$$

which takes a value 300.000 km/s for vacuum.
A similar derivation for nonhomogeneous medium yields:

$$\nabla^2 \mathbf{E} = me \frac{\partial^2 \mathbf{E}}{\partial t^2} + ms \frac{\partial \mathbf{E}}{\partial t} \tag{2.21}$$

and

$$\nabla^2 \mathbf{B} = me \frac{\partial^2 \mathbf{B}}{\partial t^2} + ms \frac{\partial \mathbf{B}}{\partial t} \tag{2.22}$$

In one dimension, Eq. 2.17 becomes (note that **E** turns into a scalar in this case):

$$\frac{\partial^2 E}{\partial x^2} = me \frac{\partial^2 E}{\partial t^2} \tag{2.23}$$

The solution to Eqs. 2.23 are in the following form: (note that propagating in x dimension)

$$E(x,t) = E_0 e^{i(kx - wt)} \tag{2.24}$$

If these solutions are used in classical wave equations, we can see that *k* is the complex wave number according to the following equation.

$$k^2 = mew^2 + ims w \tag{2.25}$$

Taking the square root of this expression, the complex wave number is written as:

$$k = k_+ + ik_- \tag{2.26}$$

where

$$k_\pm = w\sqrt{\frac{me}{2}}\sqrt{\sqrt{1+\left(\frac{s}{ew}\right)^2} \pm 1} \tag{2.27}$$

The imaginary part of the wave number k_- indicates a wave fading, i.e.

$$E(x,t) = E_0 e^{-k_x} e^{i(k_+ x - wt)} \tag{2.28}$$

$$B(x,t) = B_0 e^{-k_x} e^{i(k_+ x - wt)} \tag{2.29}$$

The *penetration depth* is defined as:

$$d = \frac{1}{k_-} \tag{2.30}$$

The real part of *k* establishes *wavelength* λ, *velocity v*, and *refractive index n*:

$$l = \frac{2p}{k_+}, v = \frac{w}{k_+}, n = \frac{ck_+}{w} \tag{2.31}$$

For a medium that conducts poorly:

$$s << we \tag{2.32}$$

In this case, penetration depth is independent of the power and the below relationships hold:

$$k_+ \square w\sqrt{me}, \quad k_- \square \frac{ms w}{2} \tag{2.33}$$

On the other hand, for a good conductor:

$$s >> we \tag{2.34}$$

In this case, k_+ and k_- become nearly equal to each other and the relationship can be expressed as in the following form:

$$k_+ \approx k_- \approx \sqrt{\frac{msw}{2}} \tag{2.35}$$

The penetration depth decreases with increasing frequency in good conductors. Also, the value of *s* and *e* may depend on the frequency. It is known that some media can be a good conductor at lower frequencies and a bad conductor at higher frequencies.

At GSM frequencies, human tissues, in general, have intermediate (i.e. neither good nor bad) conductivities. According to the classical wave equation's solution, it is understood clearly that the penetration depth of EM wave propagating in a conductive media is changed with conductivity (σ), dielectric properties (ε), magnetic properties (m), frequencies (f) and no changed with the power (P).

Eq. 2.17 can be rewritten by arranging the second order time derivative term on the right. Assuming a sinusoidal wave, **E** can be written as $\mathbf{E}(x,y,z,t) = \mathbf{E}(x,y,z)e^{iwt}$ and Eq. 2.17 becomes:

$$\nabla^2\mathbf{E} = m_0 e_0 \frac{\partial^2\mathbf{E}}{\partial t^2} = im_0 e_0 w \frac{\partial\mathbf{E}}{\partial t} = -m_0 e_0 w^2\mathbf{E} \tag{2.36}$$

Thus,

$$\nabla^2\mathbf{E} + m_0 e_0 w^2\mathbf{E} = 0 \tag{2.37}$$

$$\nabla^2\mathbf{E} + k^2\mathbf{E} = 0 \tag{2.38}$$

For conductive media,

$$\nabla^2\mathbf{E} + (emw^2 - ims w)\mathbf{E} = 0 \tag{2.39}$$

Eq. 2.39. can be arranged by using Eq. 2.21. as below:

$$\nabla\times\nabla\times\mathbf{E} - emw^2\mathbf{E} + ims w\mathbf{E} = 0 \tag{2.40}$$

$$\nabla\times\nabla\times\mathbf{E} - \left[\frac{e_0 emw^2}{e_0}\right]\mathbf{E} + \left[\frac{ims w^2 e_0}{e_0}\right]\mathbf{E} = 0 \tag{2.41}$$

$$\nabla\times\nabla\times\mathbf{E} - e_0 mw^2\mathbf{E}\left[\frac{e}{e_0} - \frac{is}{we_0}\right] = 0 \tag{2.42}$$

For the conductivity doesn't exist in the vacuum so $k_0 = k_+$ is defined and we take $m_r = 1$,

$$\nabla\times\nabla\times\mathbf{E} - k_0^2\left[e_r - \frac{is}{we_0}\right]\mathbf{E} = 0 \tag{2.43}$$

Eq. 2.38 is known as *homogeneous Helmholtz Equation* and Eq. 2.43. is known as *nonhomogeneous Helmholtz Equation.* Notice that both equations are time-independent and frequency-dependent. These frequency-domain equations are solved with FEM.

2.3. Bioheat Transfer Equation

Heat can be transferred by three distinct mechanisms: conduction, convection and radiation. *Conduction* is a process in which heat transfer is induced by molecular diffusion. A molecule at higher temperature possesses a higher kinetic energy and thus is in a more excited state. The molecule transmits part of energy to its neighboring molecule at a lower energy level. *Convection* is a process in which heat is transferred by the simultaneous action of molecular diffusion and mixing motion. It takes place only in fluids. Radiation is a process in which heat is transferred by electromagnetic wave phenomena. It occurs in vacuum space, in fluids as well as in solids.

The *bioheat equation* is most commonly used equation for regional variations in temperature and heat flux in living tissues. It originates from the conservation of the thermal energy.

$$r c_p \frac{\partial T}{\partial t} + w_b c_{pb}(T - T_A) = k\left(\frac{\partial^2 T}{\partial x^2} + \frac{\partial^2 T}{\partial y^2} + \frac{\partial^2 T}{\partial z^2}\right) + q_m + q_r \qquad (2.44)$$

In Eq. 2.44, $\frac{\partial T}{\partial t}$ is the time rate of change of the temperature which vanishes at steady state. r and c_p are the density and specific heat, respectively, of the tissue. $w_b c_{pb}(T - T_A)$ indicates the convective heat transfer, i.e. the heat brought or carried away by the blood flow through the tissue. In this term, w_b and c_{pb} are the perfusion rate and the specific heat, respectively, of the blood which enters the tissue with an arterial temperature of T_A. $k\left(\frac{\partial^2 T}{\partial x^2} + \frac{\partial^2 T}{\partial y^2} + \frac{\partial^2 T}{\partial z^2}\right)$ is the conductive heat transfer to the tissue with k indicating the conductivity of the tissue. q_m is metabolic heat generation and q_r refers to the radiation heat transfer which is typically negligible at low temperatures such as the body temperature. (Yang, 1989)

2.4. Coupling of the Equations, Specific Absorption Rate (SAR)

Electromagnetic absorption in tissue results to the generation of thermal energy (i.e. heating) of the tissue, quantified by the specific absorption rate (SAR). SAR is defined as (Morega M et al, 2011):

$$SAR = \frac{s \cdot \left|\mathbf{E}_{rms}\right|^2}{r} \tag{2.45}$$

where σ, ρ are the electric conductivity and density, respectively, of the tissue. $\mathbf{E}_{rms}$ is the root mean square of the electric field.

SAR can be considered as an additional heat generation term and put into the bioheat transfer equation:

$$r c_p \frac{\partial T}{\partial t} + w_b c_{pb}(T - T_A) = k\left(\frac{\partial^2 T}{\partial x^2} + \frac{\partial^2 T}{\partial y^2} + \frac{\partial^2 T}{\partial z^2}\right) + q_m + r \cdot SAR \tag{2.46}$$

Eq. 2.46 reflects the coupling of the Helmholtz and bioheat transfer equations. At steady state, the SAR term will take a constant value and it can be lumped with the metabolic heat generation term q_m.

3. FINITE ELEMENT METHOD (FEM) FOR ELECTROMAGNETICS

FEM has been in use for solving electromagnetic problems almost for 45 years. FEM is preferable for the solution of problems defined on irregular geometries. The FEM analysis involves four basic steps:

(a) Discretizing the problem region into a finite number of sub regions or elements;
(b) Forming a weak form of the mathematical problem at hand and evaluating this on each element to build element matrices
(c) Assembling of all element matrices to a global system of equations;
(d) Solving the system of equations.

Finite elements method's simplest sub domains in one, two, three dimensional space are line elements, triangles and tetrahedrons, respectively. Other elements like rectangular patches, bricks etc. are also used Fig 5.

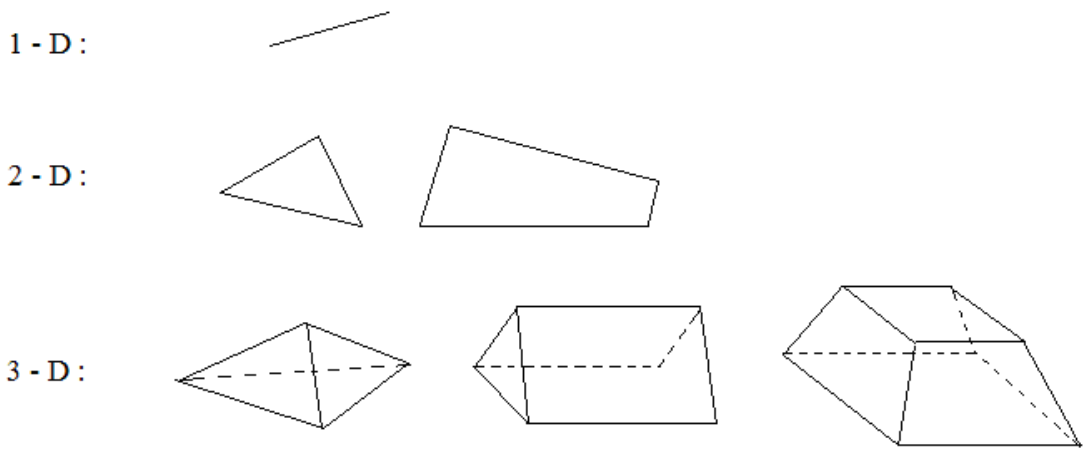


Figure 5. Basic Finite Elements: 1-D: Line element, 2-D: Triangle, Quadrilateral and 3-D: Tetrahedron, Pentahedron and Hexahedron.

3.1. Method of Weighted Residuals

FEM can be considered as a specific type of *method of weighted residuals*, a general approximation methodology used in the solution of differential equations.

The finite element package, COMSOL (see Chapter 4 for details) used in this study, does not provide the details of the finite element formulation used to solve the problem at hand. Hence, we outline here briefly how the FEM is derived from a weighted residual approach for a general differential equation. The details of general FEM method can be found in any related textbook **(**Tak et al, 1996 , Polycarpou, 2006)

Suppose that the following differential equation holds for a field variable q :

$$\mathrm{A}(q) - b = 0 \tag{3.1}$$

where q is solution to the equation and A is a differential operator operating on q . The function b is a known function in the problem domain Ω which is bounded by the boundary surface Γ. Proper boundary conditions are prescribed on Γ. In FEM, we look for an approximate solution $\bar{q}$ to the problem in the form

$$q \approx \bar{q} = \sum_{i=1}^{n} q_i \cdot N_i \tag{3.2}$$

where N_i are basis functions belonging to certain functions space (such as the set of all piecewise linear functions) defined over the problem domain Ω. q_i are the unknown variables and n is the number of unknowns. Eq. 3.2 is substituted into Eq. 3.1 giving

$$\mathrm{A}(\bar{q}) - b = r \tag{3.3}$$

where r is the resulting error due to the approximate nature of $\bar{q}$, called the *residual*. In the method of weighted residuals, the residual term, Eq. 3.3, is multiplied with a weighting function W belonging to a certain space of functions, integrated over the problem domain and set to be equal to zero.

$$\int_{\Omega} r \cdot W d\Omega = 0 \text{, i = 1,2…,n} \tag{3.4}$$

The unknowns q_i are determined such that Eq. 3.4 holds for any choice of W from the designated function space.

If N and W are chosen to belong to the same function space (such as the set of piecewise linear functions which is a very popular choice in FEM), the problem formulation is called a *Galerkin* formulation.

3.2. Boundary and Interface Conditions

To solve the 3-D electromagnetic problem, we also need the specify boundary conditions at material interfaces and physical boundaries. At interfaces between two media, the boundary conditions can be expressed mathematically as: (Comsol)

$$\mathbf{n}_2 \times (\mathbf{E}_1 - \mathbf{E}_2) = \mathbf{0} \tag{3.5}$$

$$\mathbf{n}_2 \cdot (\mathbf{D}_1 - \mathbf{D}_2) = r_s \tag{3.6}$$

$$\mathbf{n}_2 \times (\mathbf{H}_1 - \mathbf{H}_2) = \mathbf{J}_s \tag{3.7}$$

$$\mathbf{n}_2 \cdot (\mathbf{B}_1 - \mathbf{B}_2) = 0 \tag{3.8}$$

where ρ_s and J_s denote surface charge density and surface current density, respectively and n_2 is the outward normal from medium 2. A consequence of the above is the interface condition for the current density.

$$\mathbf{n}_2 \cdot (\mathbf{J}_1 - \mathbf{J}_2) = -\frac{\partial r_s}{\partial t} \tag{3.9}$$

3.3. Perfectly Matched Layers (PMLs) in the Models

It's very important treat that there are a lot of open boundaries in the radiation problem. In Comsol, the RF module offers two closely related types of absorbing boundary conditions. These are the scattering boundary conditions and the port boundary conditions. The scattering boundary condition is a first order absorbing boundary condition for a plane wave or a cylindrical or spherical wave, whereas a port boundary condition is a perfectly absorbing condition for general modes of a known shape, provided that the correct mode shape and the propagation constant are supplied. Several port boundary condition features representing an expansion into mutually orthogonal modes are also allowed and can be used to account for higher diffraction orders from a grating or to truncate a waveguide operated in the multimode regime. However, in many scattering and antenna-modeling problems, you cannot describe the outgoing radiation as a plane wave with a well-known direction of propagation or as a known, finite modal expansion. In such situations, consider using perfectly matched layers (PMLs).

The PML formulation can be deduced from Maxwell's equations by introducing a complex-valued coordinate transformation under the additional requirement that the wave impedance should remain unaffected.

In this study, the RF module uses the following coordinate transform for the general coordinate variable, t.

$$t' = \left(\frac{t}{\Delta_w} \right)^n \cdot (1-i) \cdot l \cdot F \tag{3.10}$$

The coordinate, *t*, and the width of the PML region, Δ_w, are geometrical parameters that are automatically extracted for each region. The other parameters are the PML scaling factor F and the PML order n that can be modified in the PML feature (both default to unity). To avoid a non-linear dependence in the eigenvalue, the wavelength, λ, is removed from the scaling expression when computing an eigenfrequency study. The software automatically computes the value for Δ_w and the orientation of the transform for PML regions that are cartesian, cylindrical, or spherical.

The used PML of the studied model is shown in Fig 6.

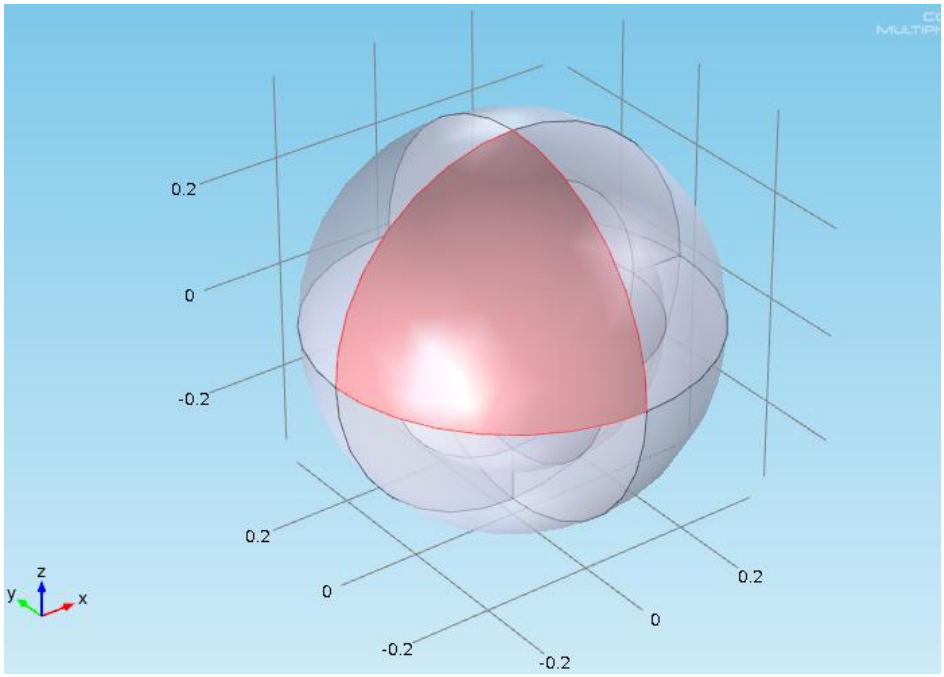


Figure 6. An example picture of finite PML in the problem space surface model.

4. GEOMETRIC MODELS

4.1. Introduction

It is important that the differential equation is solved on a realistic geometry for successful simulation of the considered phenomenon. Typically, the creation of the geometric model representing the FEM problem domain is a separate and independent process. Solid modeling softwares are available to create geometric models which are imported by the FEM software for analysis.

In this study, two head models are utilized. The first one is a homogeneous head model available in the COMSOL library. The second one is a nonhomogeneous head model which is created from MRI data as described below.

4.2. The Homogeneous Head Model

The homogeneous human head model provided by COMSOL software originates from the so-called Specific Anthropomorphic Mannequin (SAM) Phantom of IEEE, IEC, and CENELEC from their standard specification of SAR value measurements. The computer model of this head phantom is obtained from a MRI image (Fig. 7) containing 109 slices, each with 256 x256 voxels (Comsol tutorial). The resulting model (Fig. 8) has realistic physical dimensions (Table 4.1).

The antenna model (see section 4.4) is separate from the head model. In order to combine both models in one computational domain, the surrounding air is also added into problem domain in a spherical geometry (Fig. 9). The views of the computational domain along the three Cartesian coordinate axes are shown on Figs. 10-12.

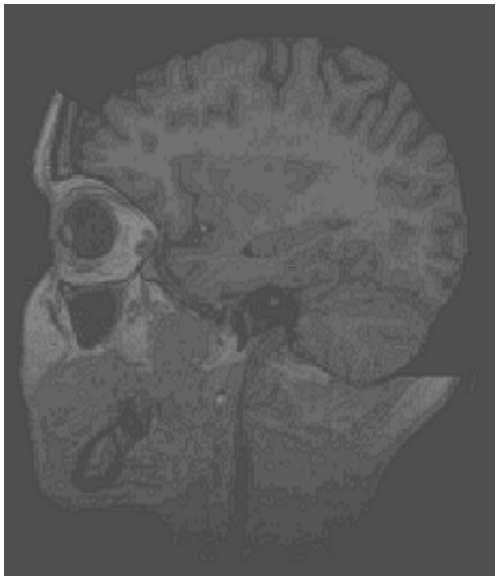


Figure 7. An example of MRI pictures used in homogeneous head model.

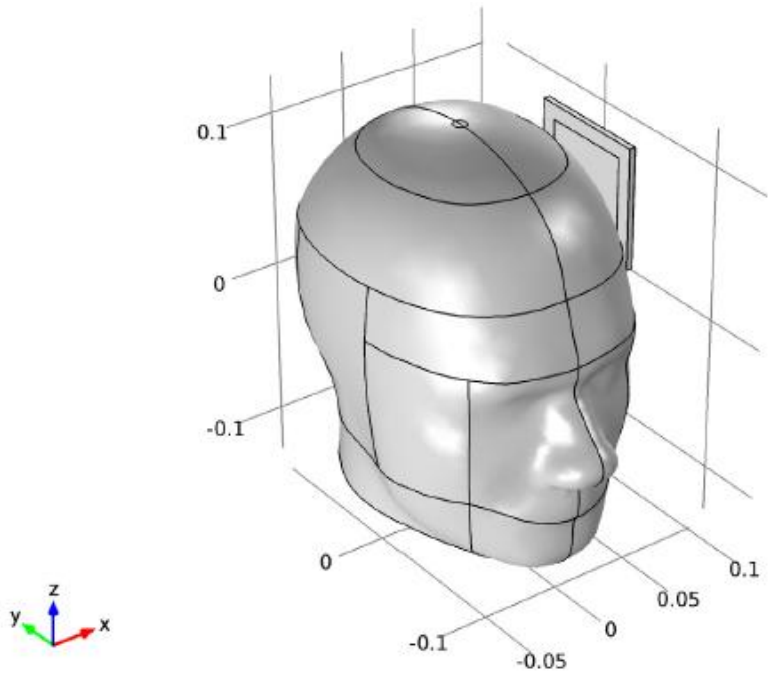


Figure 8. The homogeneous FEM head and patch antenna model in realistic dimensions.

Table 4.1. The dimensions of homogeneous head model.

	Homogeneous head model	
Head dimensions (cm)	x	16
	y	18.8
	z	23.7

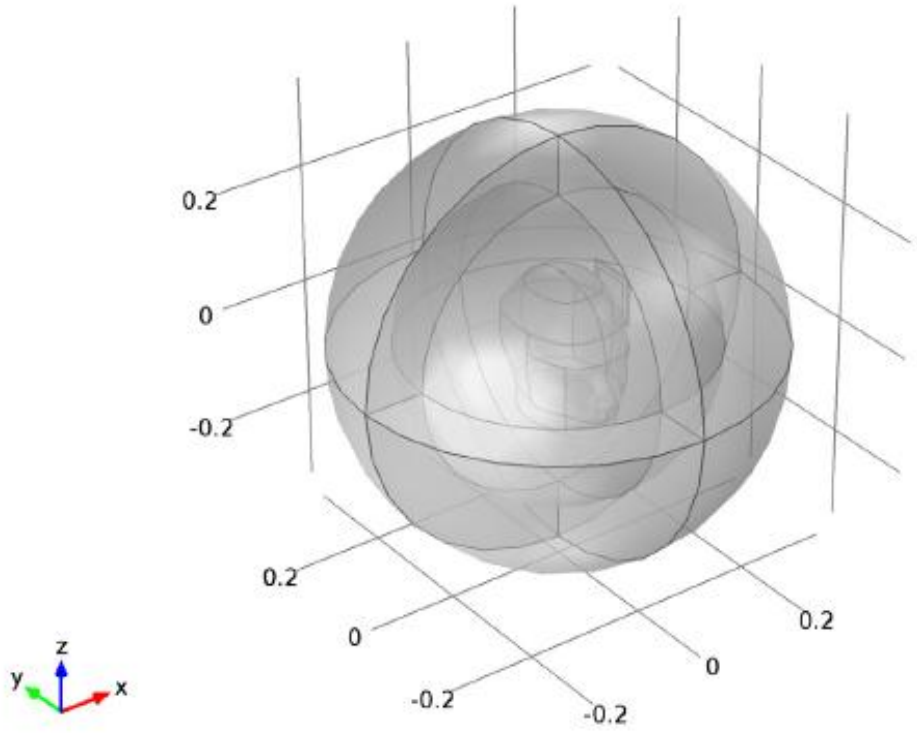


Figure 9. The numeric FEM head and patch antenna model in realistic dimensions.

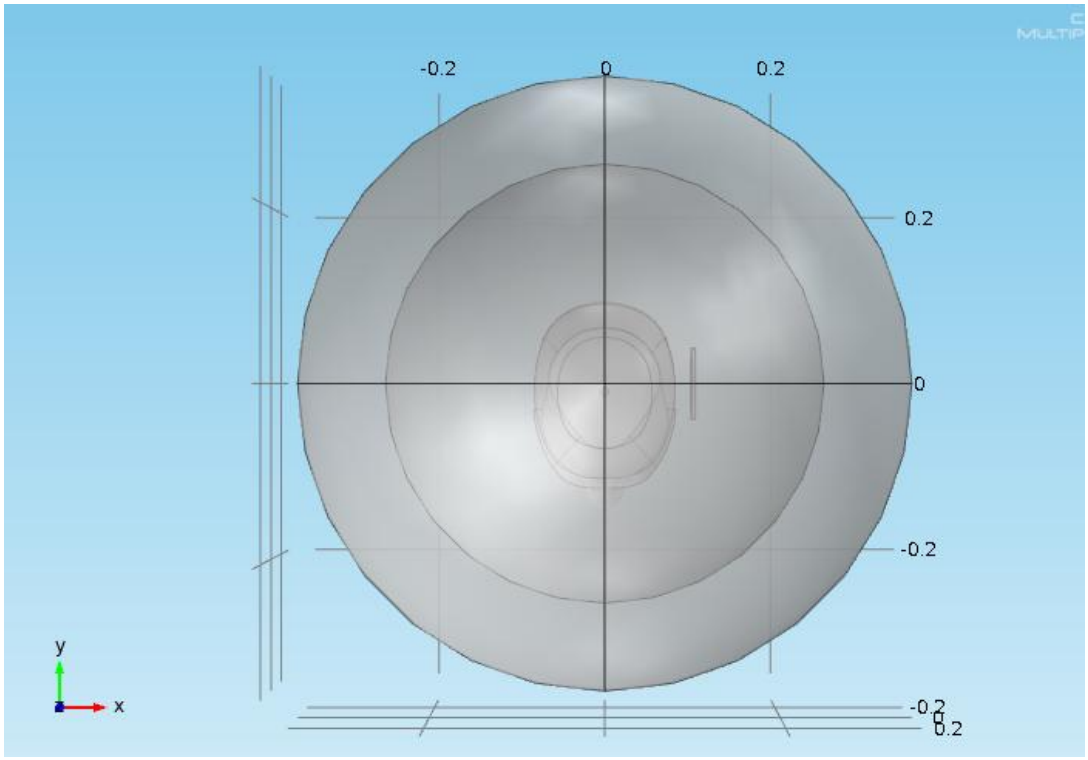


Figure 10. The view of the problem space along the z-axis.

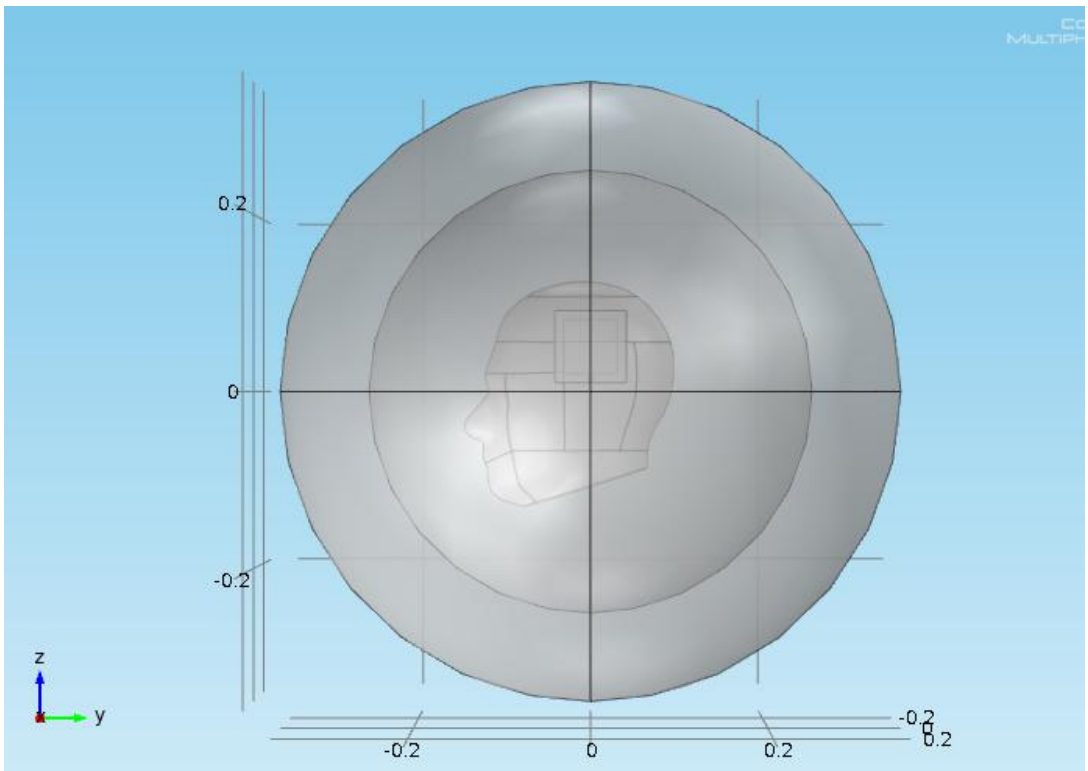


Figure 11. The view of the problem space along the x-axis.

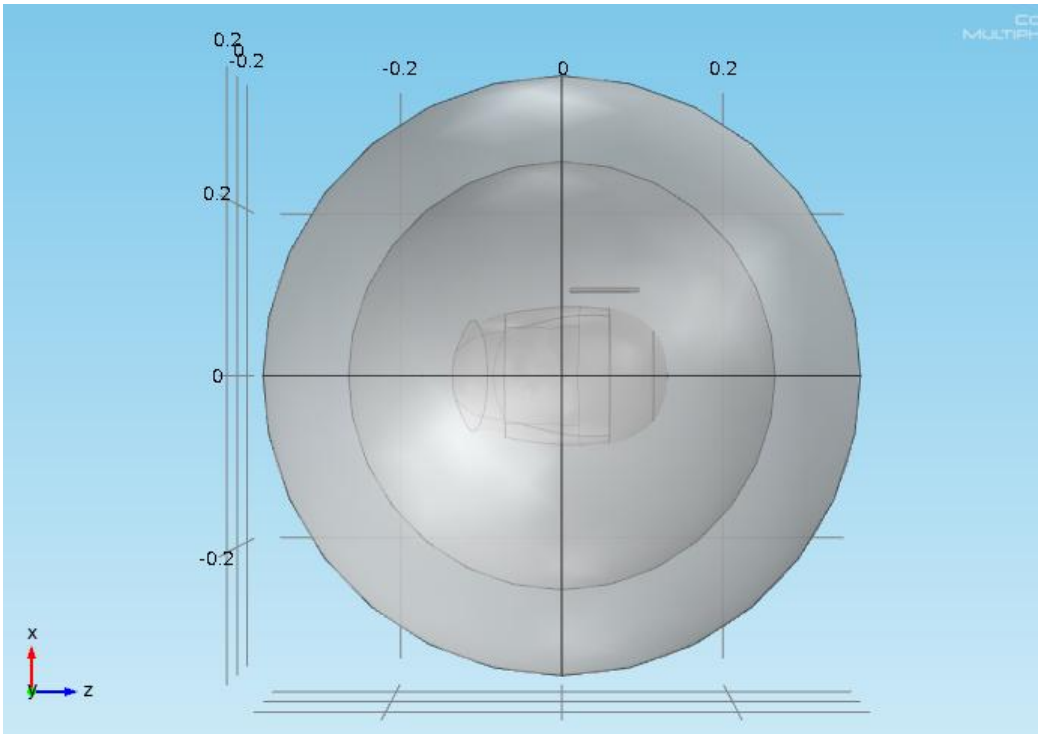


Figure 12. The view of the problem space along the y-axis.

4.3. A Nonhomogeneous Realistic Head Model

A significant amount of work is dedicated to forming a realistic head model in this study. While certain models were available through internet resources, many of these models had issues regarding their transfer to the FE environment. Some models were just shell models which were hollow inside, while other models were available in formats that are not compatible with typical FE environments. As a result, we had to create a head model from scratch using the slice data of a partial head model, involving the middle part of the head, available in MIMICS software (Materalise Nv. Mimics software).

Totally, 90 MRI pictures are used to create the realistic head model. A total of 930 appearances of the 3D head model are manipulated (Figs. 13-15). Certain unwanted artifacts are removed and holes that form in the model during the reconstruction are patched to obtain the final model (Fig. 16).

While not ideal, the partial nature of the head model is not a crucial factor with respect to the simulation results. The missing parts are relatively distant from the part of the domain where the highest gradients occur. To partially account for the missing material, an insulation boundary condition (rather than a convective one) is imposed on the top and the bottom of the head model in the heat transfer problem.

While the head model involves a brain tissue, it is not possible to reconstruct the border of the bone and brain tissues due to the complex irregular nature of it. Instead, two concentric cylindrical surfaces of appropriate dimensions are added to the head model. As a result, the model involves three different tissues (Fig. 17): a layer which represents skin and fat (using an average of the properties of both types of tissues), underneath that the bone layer which encapsulates the brain. The computational domain for the nonhomogeneous model is shown on Fig. 18.

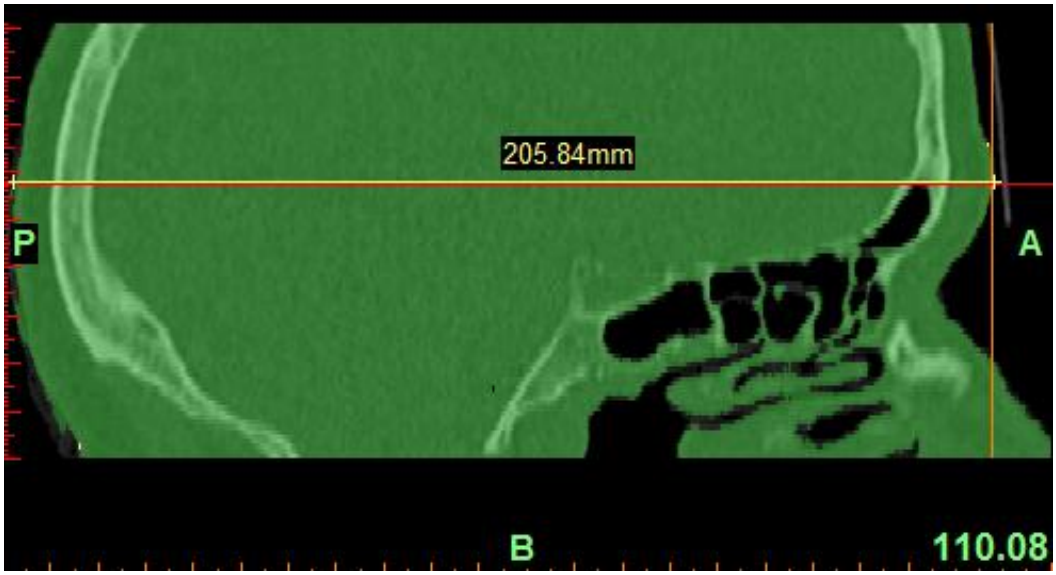


Figure 13. The size of MRI data used in FEM nonhomogeneous head model (xz direction).

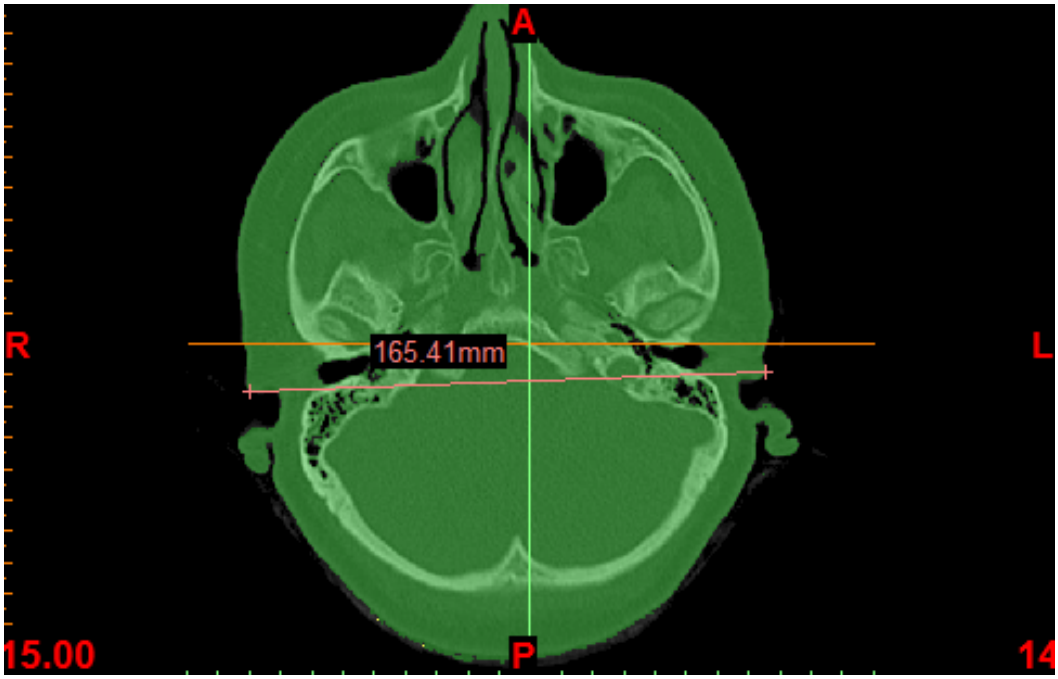


Figure 14. The size of MRI data used in FEM nonhomogeneous head model (xy direction).

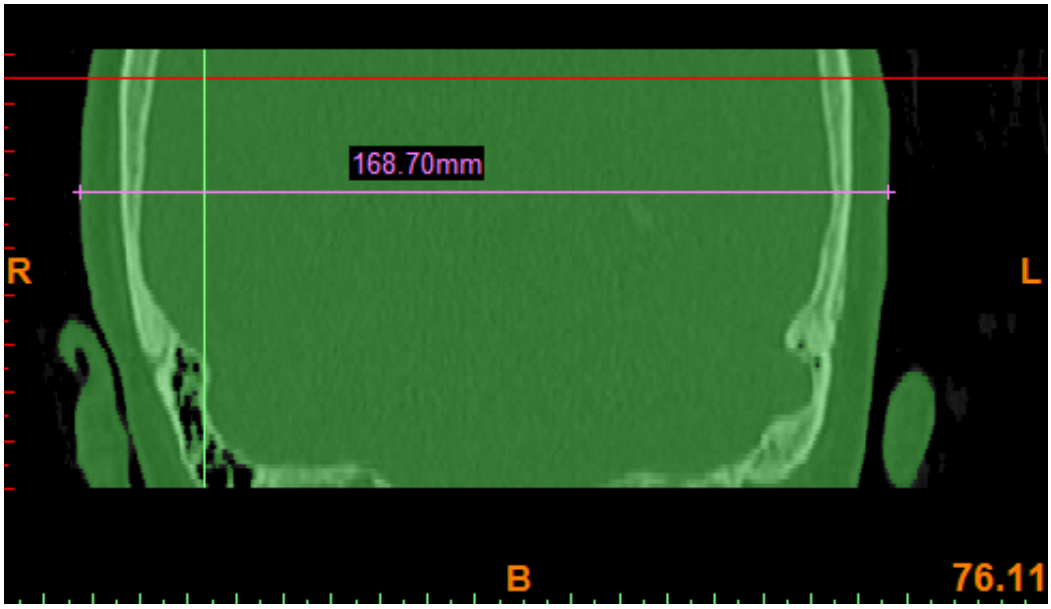


Figure 15. The size of MRI data used in FEM nonhomogeneous head model (yz direction).

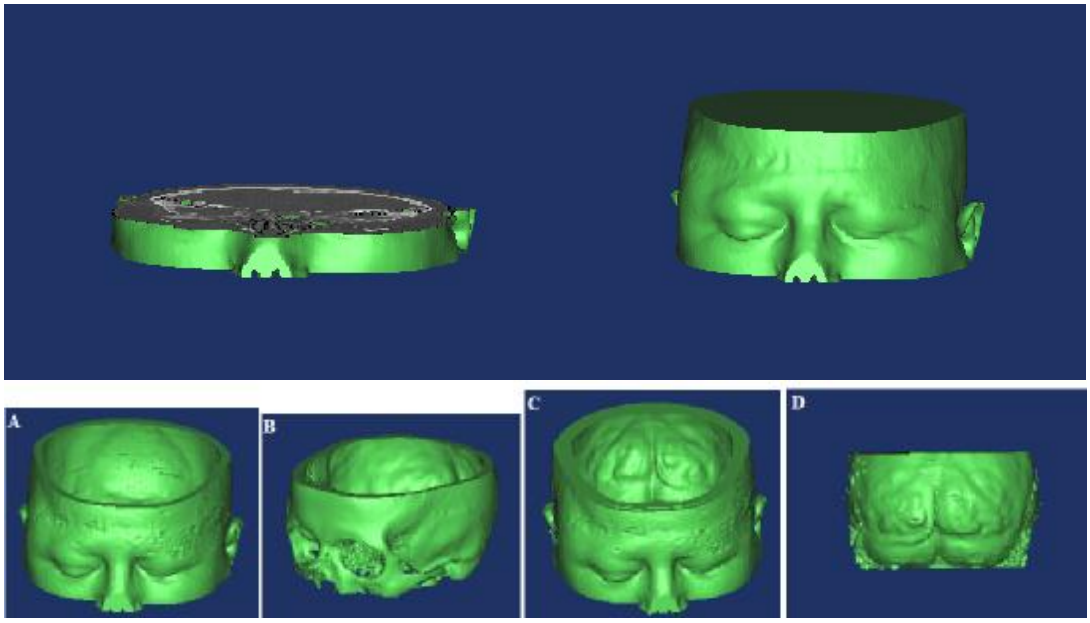


Figure 16. The views of head model's layers. (A) The skin and fat tissues are coupled. (B) The skull layer. (C) The skull, skin and fat tissues are coupled. (D) The brain layer.

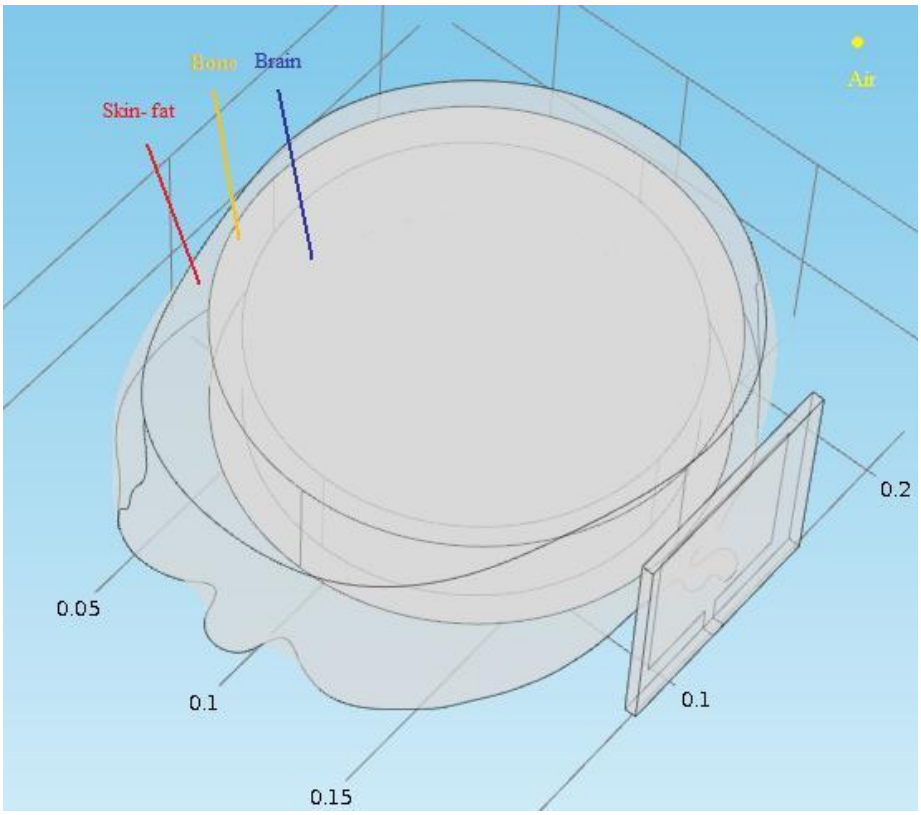


Figure 17. The head model with layers indicated.

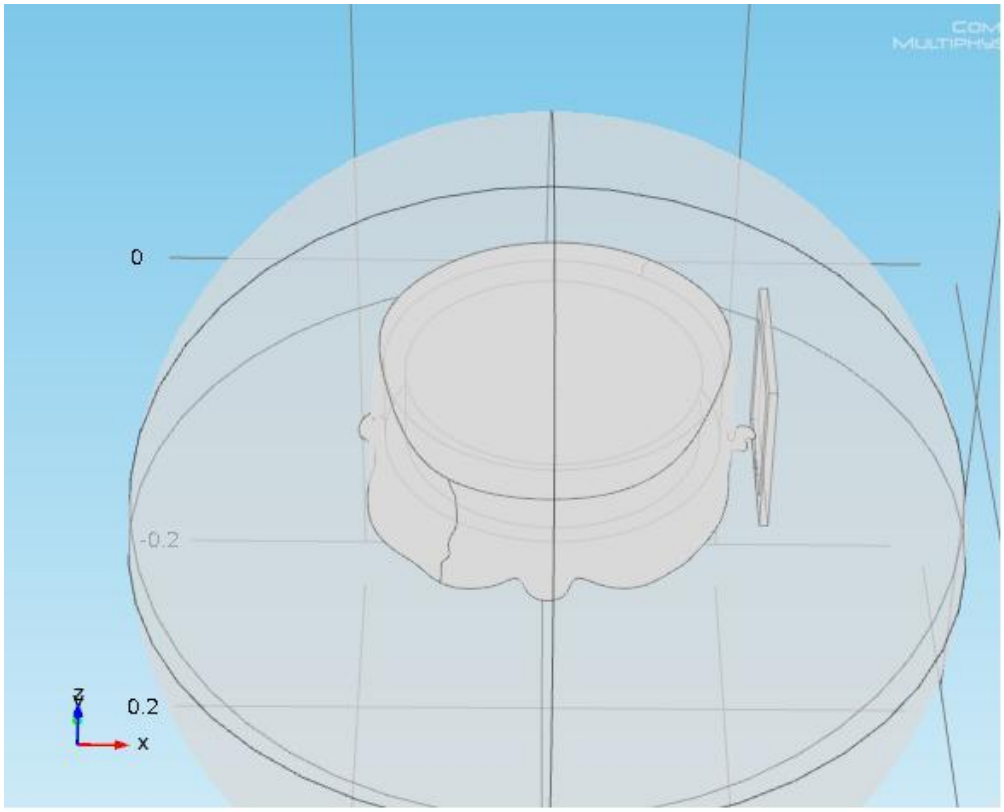


Figure 18. The general view of the problem space (Air, head model and patch antenna).

4.4 Patch Antenna Model

The homogeneous head model of COMSOL involves an antenna model which is placed with a gap to the head about 1 cm large. In our nonhomogeneous model, we placed it right next to the skin-fat tissue around the ear area to maximize its effect.

The antenna dimensions are given on Table 4.2.

Table 4.2. The antenna dimensions used in this study.

Average size of antenna (cm)	
Width	0,4
Depth	8
Height	8

5. THE NUMERICAL SIMULATION

5.1 Problem Parameters

The values of the parameters associated with the electrical and thermal problem are calculated by averaging the corresponding parameter values of skin, fat, bone and brain tissues (Wessapan et al, 2012). The definitions and numerical values of the homogeneous model parameters are given in Tables 5.1. and 5.2. The same parameters for the nonhomogeneous model are taken from the literature (Wessapan et al, 2012). The values of skin – fat tissue are averages of the related values of both tissues. The definitions and numerical values of the nonhomogeneous model parameters are given in Tables 5.3. and 5.4.

Table 5.1. Problem parameters in used program for homogeneous study at 900 MHz.

Global Definitions of the Problem	**Value**	**Description**
Epsilon r (pcb)	5,23	Permittivity of the patch antenna board
Epsilon (head)	29.833	Permittivity of the head tissue
Sigma (head)	0.52125 S/m	Conductivity for the head tissue
rho_brain	1111 kg/m^3	Density of the head tissue
c_blood	2000 J(kg*K)	Heat capacity of the blood
rho_blood	1500 kg/m^3	Density of the blood
Air pressure	1 atm	Air pressure
Air space radius	35 cm	Air space radius
Frequency	900 MHz	Frequency
Conductivity	0.4	Thermal conductivity
Perfusion rate of blood	0.0003	Perfusion rate of blood
c_head	3250	Heat capacity of head

Table 5.2. Problem parameters in used program for homogeneous study at 1800MHz.

Global Definitions of the Problem	**Value**	**Description**
Epsilon r (pcb)	5,23	Permittivity of the patch antenna board
Epsilon (head)	24.7125	Permittivity of the head tissue
Sigma (head)	0.6145 S/m	Conductivity for the head tissue
rho_brain	1111 kg/m^3	Density of the head tissue
c_blood	2000 J(kg*K)	Heat capacity of the blood
rho_blood	1500 kg/m^3	Density of the blood
Air pressure	1 atm	Air pressure
Air space radius	35 cm	Air space radius
Frequency	1800 MHz	Frequency
Conductivity	0.4	Thermal conductivity
Perfusion rate of blood	0.0003	Perfusion rate of blood
c_head	3250	Heat capacity of head

Table 5.3. Problem parameters in used program for nonhomogeneous study at 900 MHz.

Global Definitions of the Problem	**Value**	**Description**
Epsilon r (pcb)	5,23	Permittivity of the patch antenna board
Epsilon (head_mix of skin-fat)	26.37	Permittivity of the mix of skin-fat tissue
Sigma (head_mix of skin-fat)	0.49 S/m	Conductivity for the mix skin - fat tissue
rho_mix of skin-fat	1020.5 kg/m^3	Density of the mix of skin-fat tissue
c_blood	2000 J(kg*K)	Heat capacity of the blood
rho_blood	1500 kg/m^3	Density of the blood
Air pressure	1 atm	Air pressure
Air space radius	20 cm	Air space radius
Frequency	900 MHz	Frequency
Conductivity_mix of skin-fat	0.5	Thermal conductivity
Perfusion rate of blood in mix of skin-fat	0.000458	Perfusion rate of blood (based on fat)
c_head_mix of skin-fat	3300	Heat capacity of head
Epsilon (head_bone)	20.79	Permittivity of the mix of skin-fat tissue
Sigma (head_bone)	0.34 S/m	Conductivity for the mix of skin-fat tissue
rho_bone	1990 kg/m^3	Density of the mix of skin-fat tissue

Conductivity_bone	0.37	Thermal conductivity
Perfusion rate of blood in bone	0.000436	Perfusion rate of blood
c_head_bone	3650	Heat capacity of head
Epsilon (head_brain)	45.805	Permittivity of the mix of skin-fat tissue
Sigma (head_brain)	0.765 S/m	Conductivity for the mix of skin-fat tissue
rho_brain	1038 kg/m^3	Density of the mix of skin-fat tissue
Conductivity_brain	0.535	Thermal conductivity
Perfusion rate of blood in brain	0.00883	Perfusion rate of blood
c_head_brain	3650	Heat capacity of head

Table 5.4. Problem parameters in used program for nonhomogeneous study at 1800 MHz.

Global Definitions of the Problem	**Value**	**Description**
Epsilon r (pcb)	5,23	Permittivity of the patch antenna board
Epsilon (head_mix of skin-fat)	18	Permittivity of the mix of skin-fat tissue
Sigma (head_mix of skin-fat)	0.299 S/m	Conductivity for the mix of skin-fat tissue
rho_mix of skin-fat	1020.5 kg/m^3	Density of the mix of skin-fat tissue
c_blood	2000 J(kg*K)	Heat capacity of the blood
rho_blood	1500 kg/m^3	Density of the blood
Air pressure	1 atm	Air pressure
Air space radius	20 cm	Air space radius
Frequency	1800 MHz	Frequency
Conductivity_mix of skin-fat	0.5	Thermal conductivity
Perfusion rate of blood in mix of skin-fat	0.000458	Perfusion rate of blood (based on fat)
c_head_mix of skin_fat	3300	Heat capacity of head
Epsilon (head_bone)	8	Permittivity of the mix of skin-fat tissue
Sigma (head_bone)	0.16 S/m	Conductivity for the mix of skin-fat tissue
rho_bone	1990 kg/m^3	Density of the mix of skin-fat tissue
Conductivity_bone	0.37	Thermal conductivity
Perfusion rate of blood in bone	0.000436	Perfusion rate of blood
c_head_bone	3650	Heat capacity of head
Epsilon (head_brain)	53	Permittivity of the mix of skin-fat tissue
Sigma (head_brain)	1.7 S/m	Conductivity for the mix of skin-fat tissue

rho_brain	1038 kg/m^3	Density of the mix of skin-fat tissue
Conductivity_brain	0.535	Thermal conductivity
Perfusion rate of blood in brain	0.00883	Perfusion rate of blood
c_head_brain	3650	Heat capacity of head

5.2 Finite Element Mesh

Using an appropriate mesh is important for a successful simulation is calculated. In the homogeneous model, the mesh includes approximately 780.000 elements. On the other hand, the nonhomogeneous model has approximately 159.000 elements. The differences in the number of elements of both models mostly originate from the difference in the problem domain sizes. The FE mesh of the homogeneous and nonhomogeneous models (including the head, the patch antenna and air) are given in Fig. (19-23).

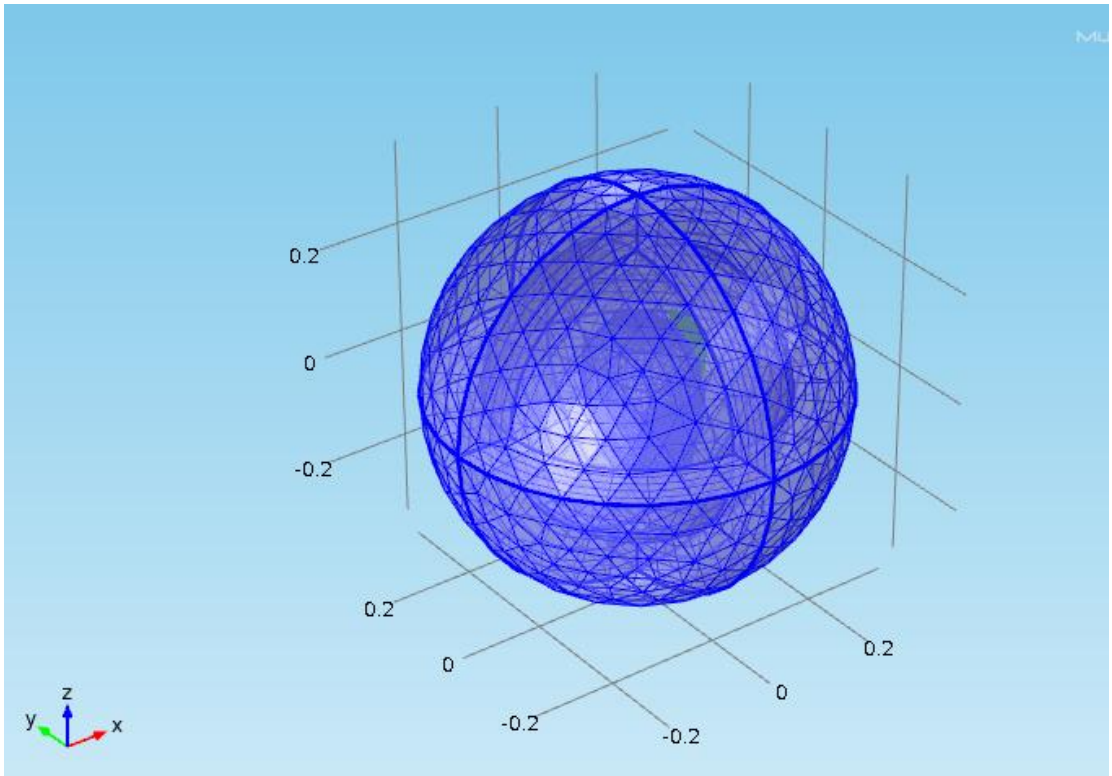


Figure 19. The finite element mesh for homogeneous head, patch antenna and air.

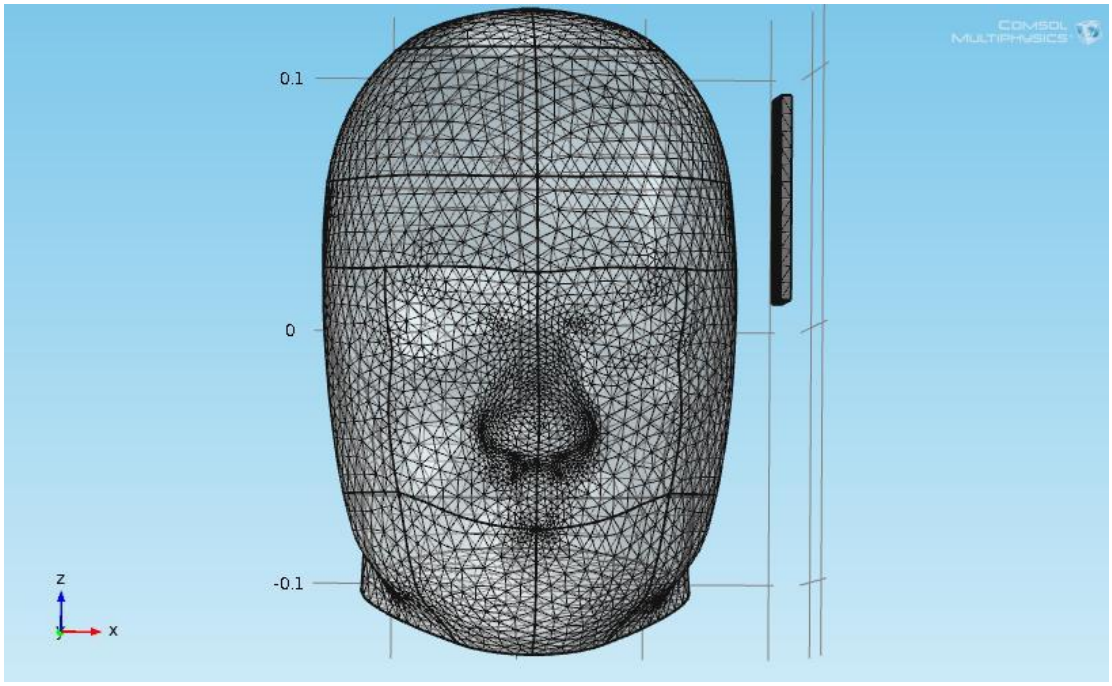


Figure 20. The picture of homogeneous head mesh space (without air)

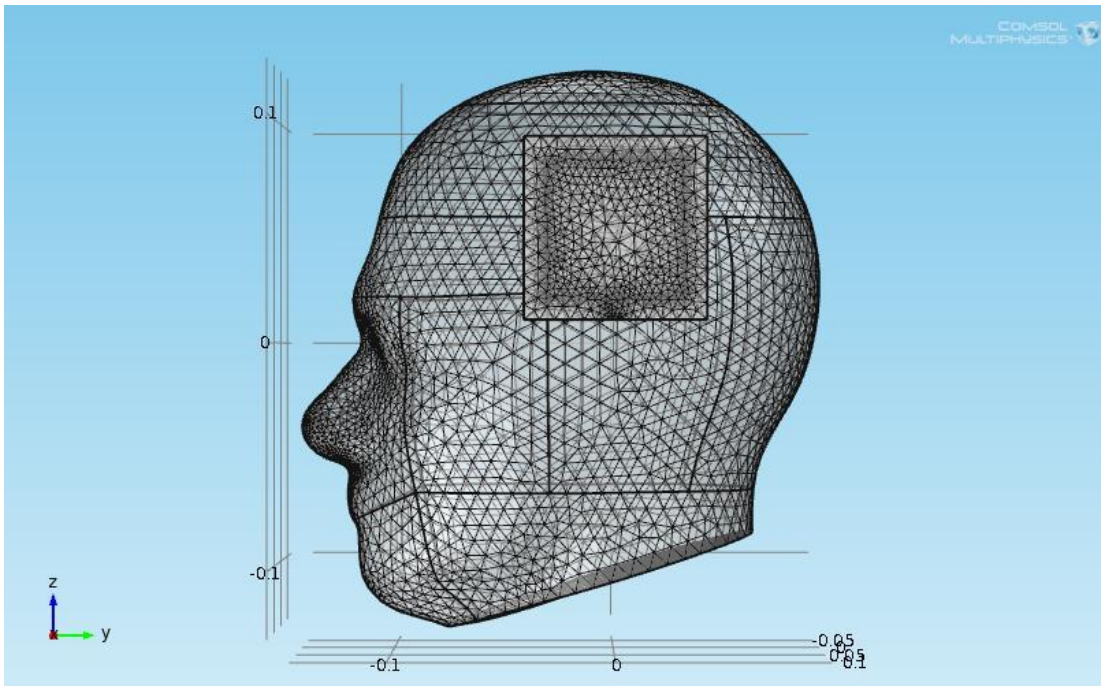


Figure 21. Another picture of head mesh space (without the surrounding air)

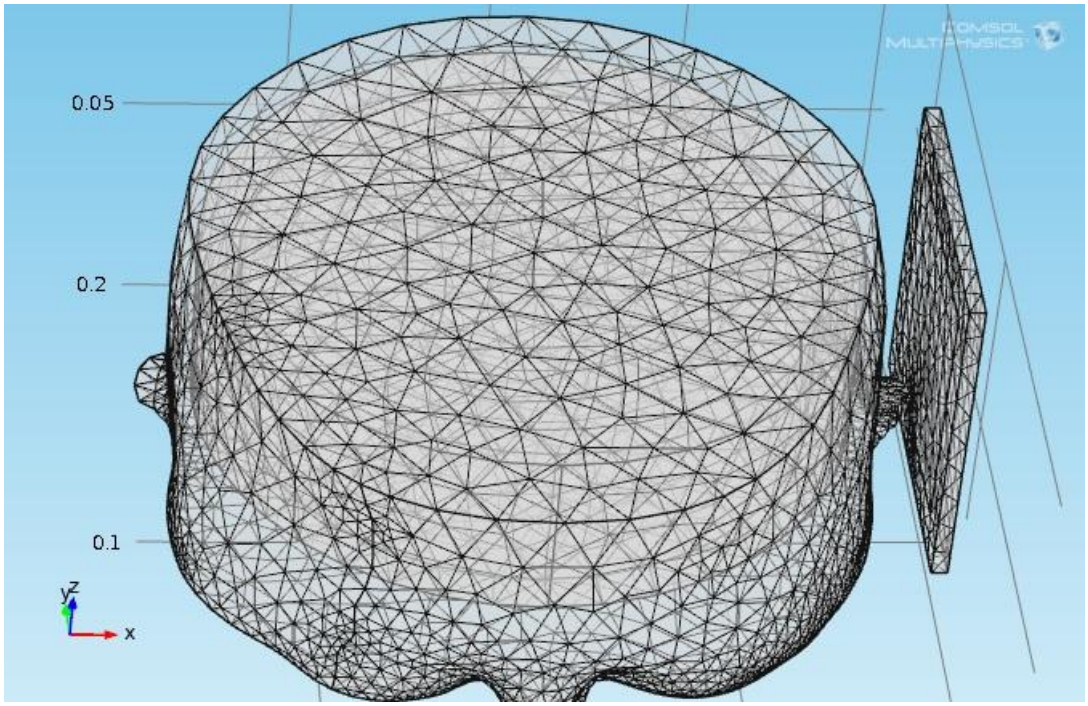


Figure 22. The finite element mesh of the head (without the surrounding air)

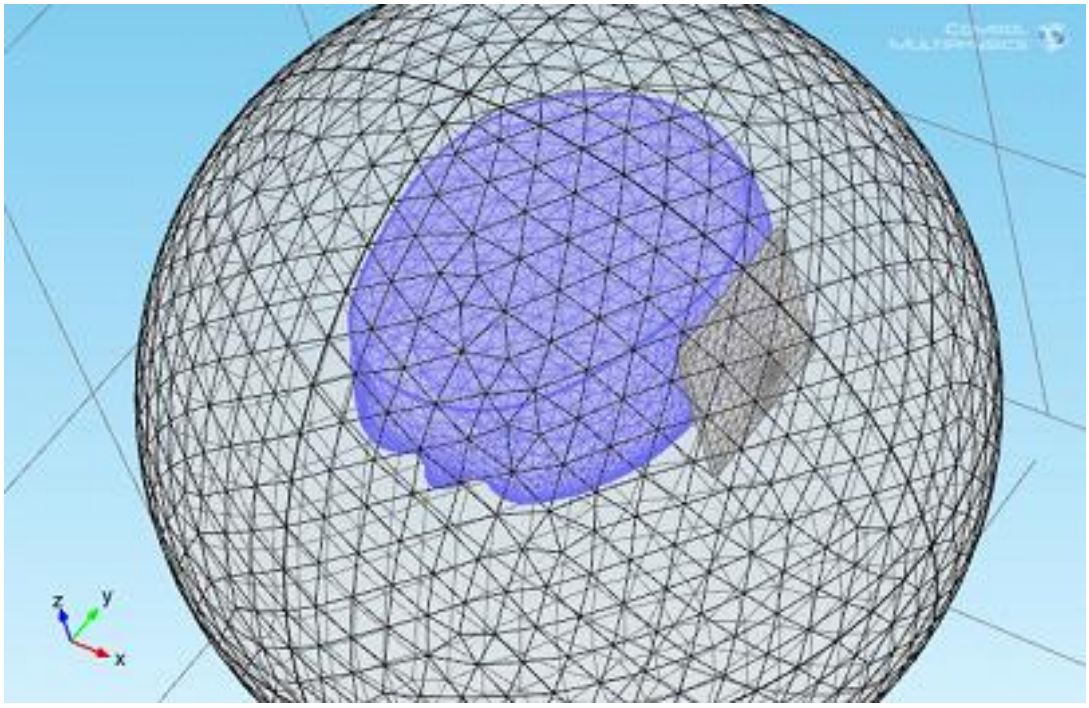


Figure 23. Another picture of realistic model's finite element mesh space.

5.3. The Analysis

The homogeneous model is analyzed at 900 and 1800 MHz frequencies with an antenna power of 0.25 W. The boundary condition (b.c.) of the heat transfer problem imposed on the side face is thermal insulation b.c. where heat is not allowed to escape from the designated boundary. The nonhomogeneous model studies are performed at 900 and 1800 MHz, with antenna powers of 0.25 and 1 W. The b.c.'s on the side face is also varied. It was either an insulation b.c. as described above or a convective cooling b.c. where heat is removed naturally by the surrounding air on the designated boundary (Table 5.5.).

Table 5.5. The conditions of studies.

	Frequency (MHz)	Power (W)	Notes
Homogeneous model	900	0.25	Thermal insulation b.c.
	1800	0.25	Thermal insulation b.c.
Nonhomogeneous model	**Frequency (MHz)**	**Power (W)**	**Notes**
	900	0.25	Convective cooling b.c.
	900	0.25	Thermal insulation b.c.
	1800	0.25	Convective cooling b.c.
	900	1	Convective cooling b.c.
	1800	1	Convective cooling b.c.
	900	1	Metabolic heat source, Convective cooling b.c.

In one analysis regarding the nonhomogeneous model, metabolic heat generation is also taken into account. Clearly, different tissues have differing metabolic rates and the experimental values proposed for these show large variations in the literature. The values used in this study are average of two sets of values taken from two different sources (T. Wessapan et al, 2011, Hirata et al, 2006) and displayed on Table 5.6.

Table 5.6. The parameter of metabolic heat source.

Metabolic heat source Q_{met} (W/m^3)	
Skin - Fat layer	400
Bone layer	300
Brain layer	5000

5.4 The Results of the Homogeneous Model

In this section, the SAR values in logarithmic scale and the temperature distributions are given for homogeneous model at 900 and 1800 MHz frequencies for 0.25 W. In the present study, the default temperature value of the body is taken 37.15 C º.

For 900 MHz case, the maximum SAR value occurring in the tissue is found to be 0.711 W/kg (Fig. 24). The maximum temperature observed in the head is 37.487 º C which reflects an increase of 0.337 º C above the baseline value (Fig. 25). The maximum electric field intensity observed in the head 55.05 V/m. The maximum SAR value increases to 0.906 W/kg if the frequency is changed to 1800 MHz (Fig. 27). The maximum electric field intensity observed in the head is 57.23 V/m. These numerical results are evaluated in detail in the next chapter.

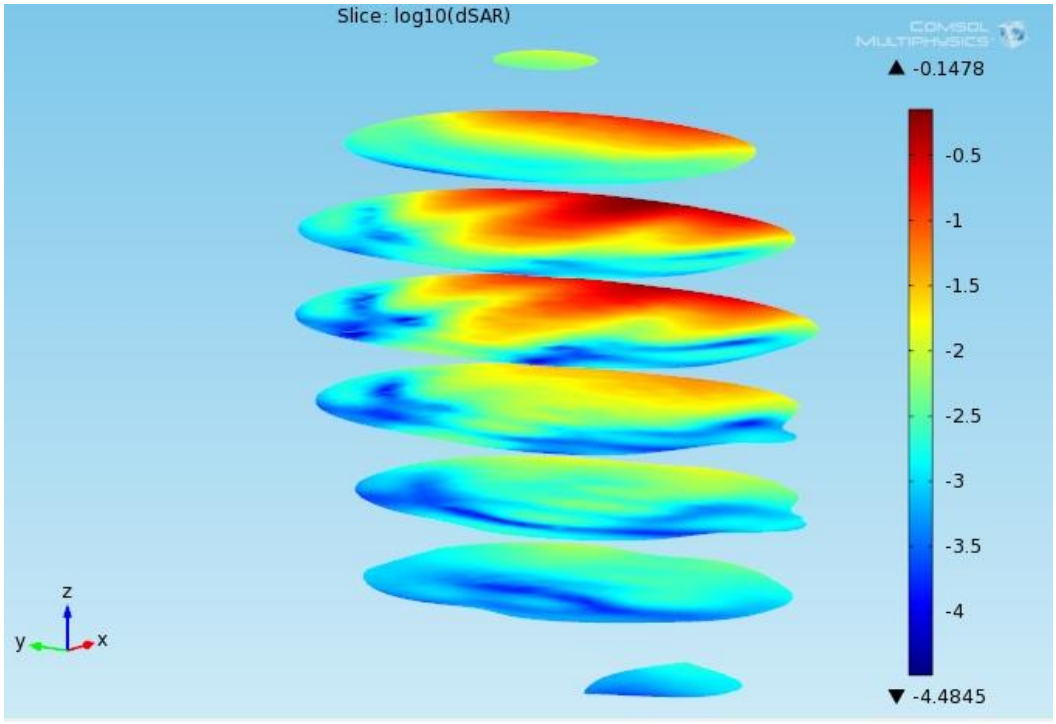


Figure 24. The log(SAR) values at 900 MHz and 0.25 W antenna power has a maximum 0.711 W/kg SAR value in homogeneous model.

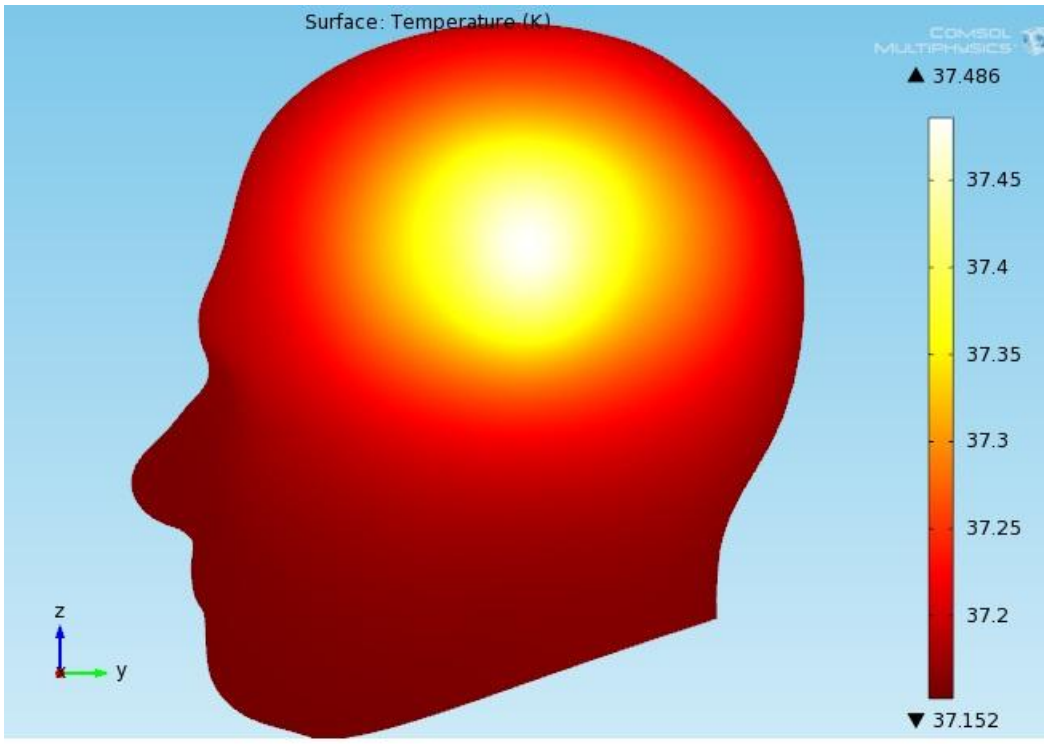


Figure 25. The local increase in surface temperature at 900 MHz and 0.25 W antenna power has a maximum 37.487 º C right beneath the antenna in homogeneous model.

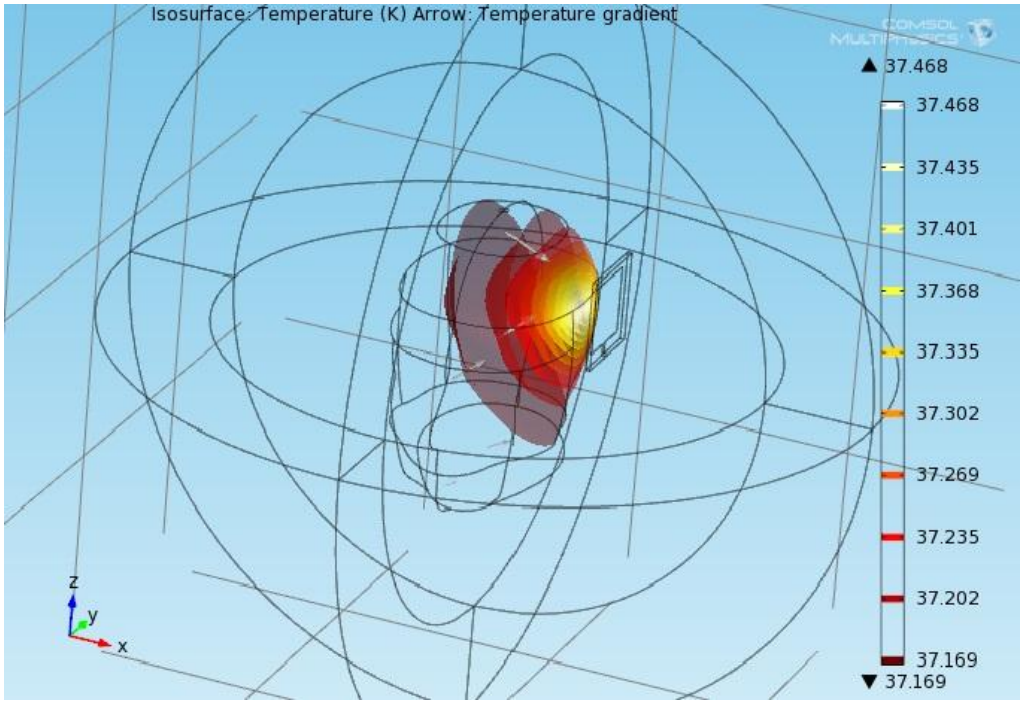


Figure 26. The isosurface temperature contours at 900 MHz and 0.25 W antenna power in homogeneous model.

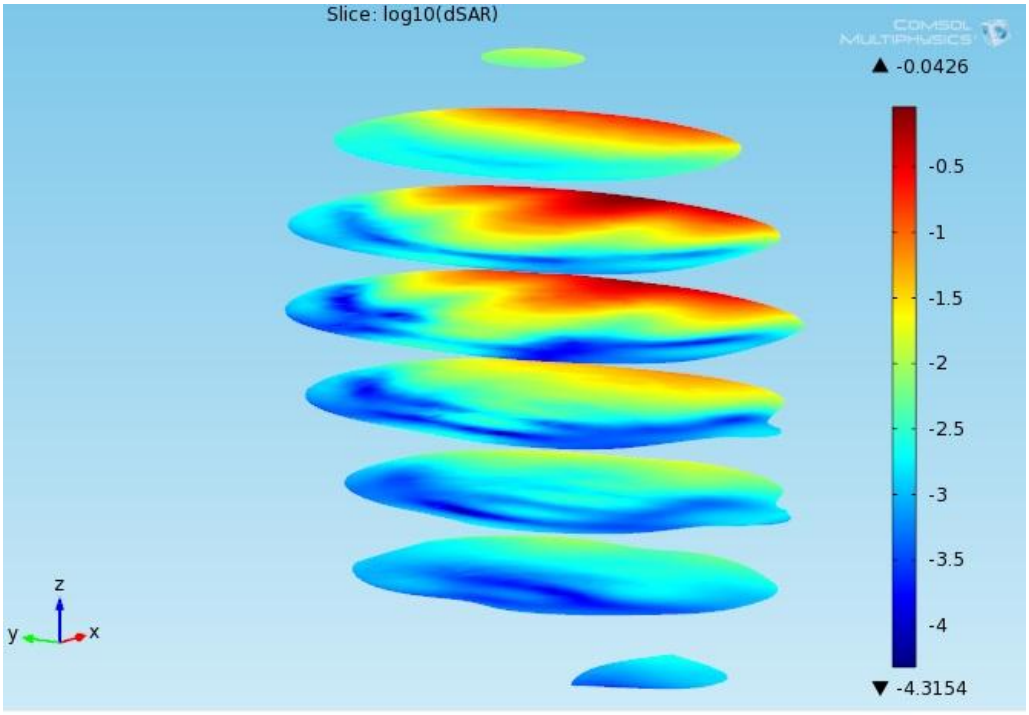


Figure 27. The log (SAR) values at 1800 MHz and 0.25 W antenna power has a maximum 0.906 W/kg SAR value in homogeneous model.

5.5. The Results of the Realistic Nonhomogeneous Model

In this section, the EM field intensity and the temperature distributions are given for nonhomogeneous model at 900 and 1800 MHz frequencies for 0.25 W and 1 W. In the present study, the default temperature value of the body is taken 37.15 C º.

For 900 MHz and 0.25 W cases, the maximum EM field intensity value occurring in the tissue is found to be 81.440 V/m (Fig. 28). The maximum temperature observed in the head is 37.277 º C (Fig. 29). The maximum temperature value decreases to 37.207 º C, if the frequency is changed to 1800 MHz (Fig. 34). For 900 MHz and 0.25 W cases, if the convective cooling b.c. is used, the temperature value changes to 37.270 º C (Fig. 31). At 900 MHz and 0.25 W, the convective cooling b.c. results to a slight decrease in maximum temperature (0.007) º C above the baseline temperature value compared to the insulation b.c. For 900 MHz and 1 W, the maximum EM field intensity value occurring in the tissue is 162.89 V/m (Fig. 36). The maximum temperature observed in the head is 37.646 º C (Fig. 37). The maximum temperature value decreases to 37.379 º C, if the frequency is changed to 1800 MHz (Fig. 40). With a metabolic heat source (Table 5.6), the temperature value and distributions are a significantly changed. For 900 MHz and 1 W case, the maximum temperature observed in the head is 37.652 º C (Fig. 42).

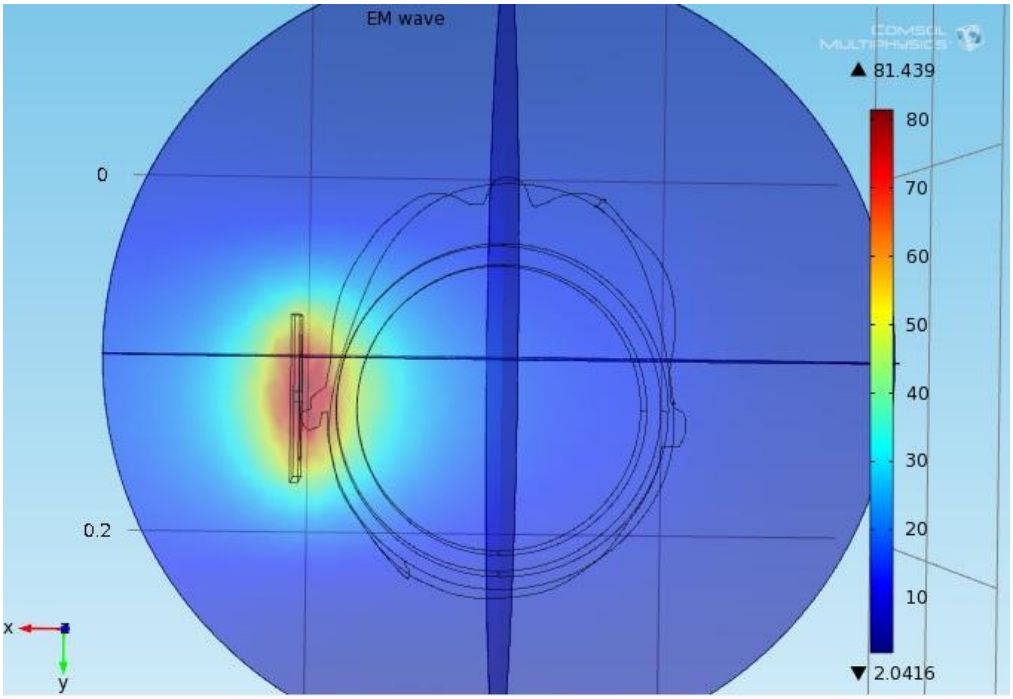


Figure 28. The EM field propagation at 900 MHz and 0.25 W antenna power has a maximum 81.440 V/m value in nonhomogeneous model.

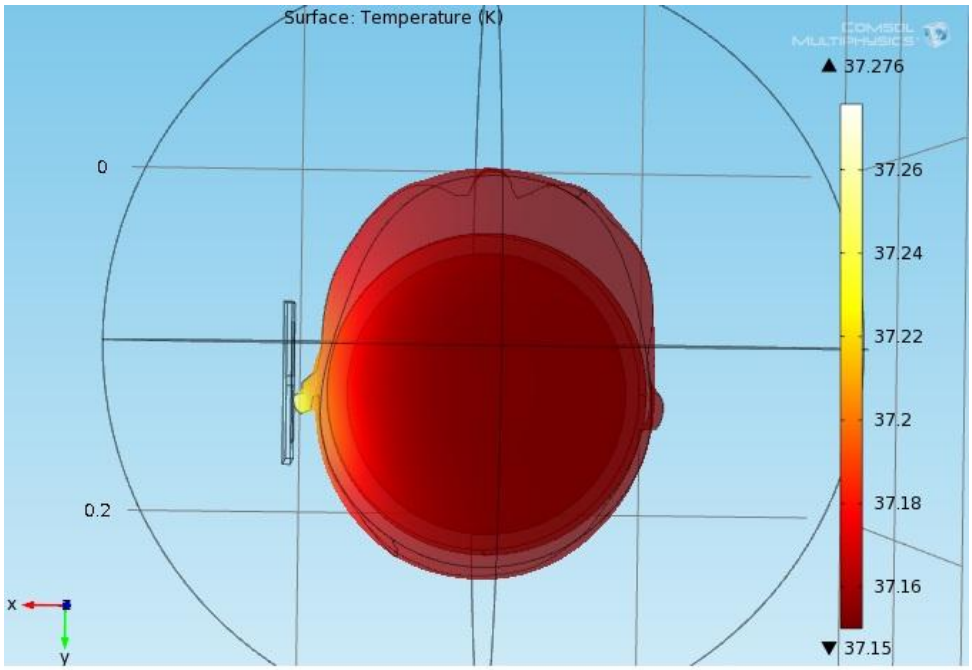


Figure 29. The local increase in surface temperature at 900 MHz and 0.25 W antenna power with thermal insulation boundary conditions has a maximum 37.276 º C right beneath the antenna in nonhomogeneous model.

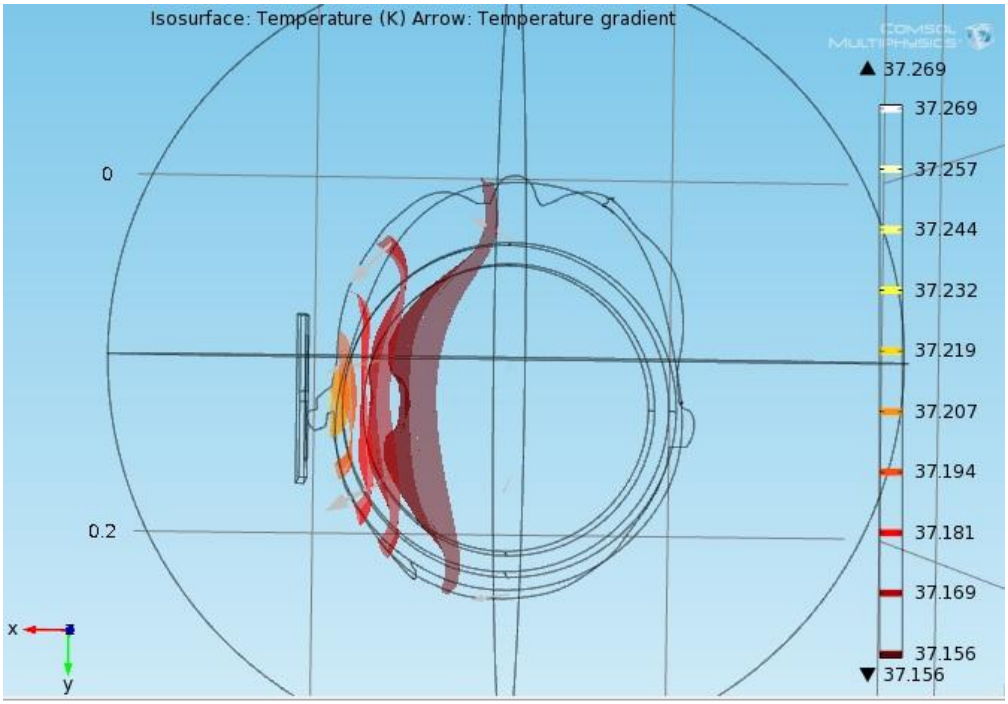


Figure 30. The contour temperature lines at 900 MHz and 0.25 W antenna power with thermal insulation boundary conditions in nonhomogeneous model.

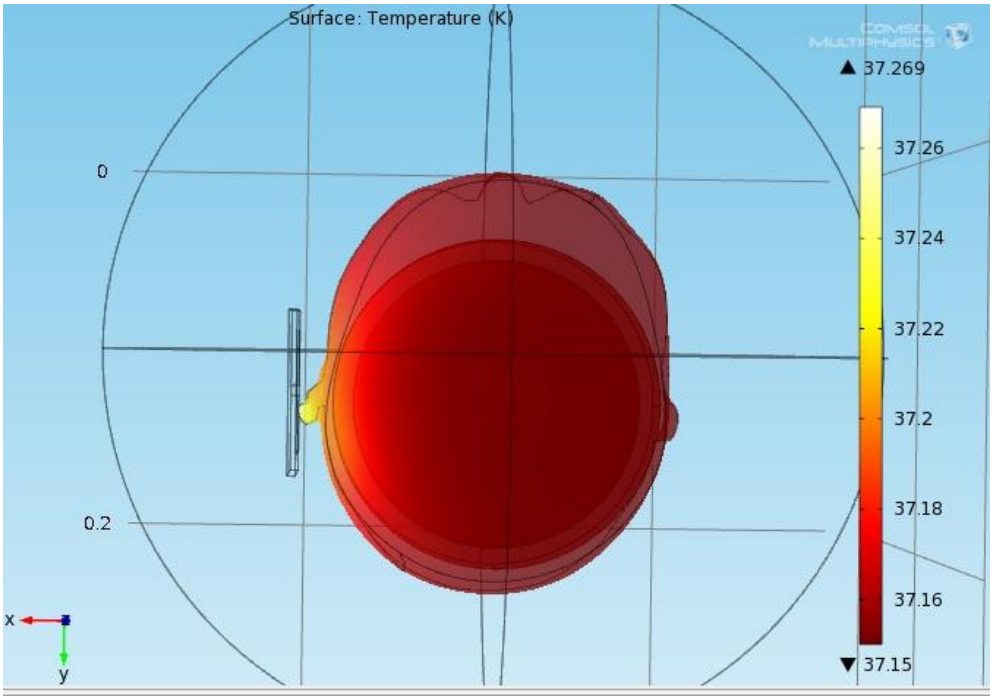


Figure 31. The local increase in surface temperature at 900 MHz and 0.25 W antenna power with convective cooling boundary conditions (h=0.666) has a maximum 37.270 ° C right beneath the antenna in nonhomogeneous model.

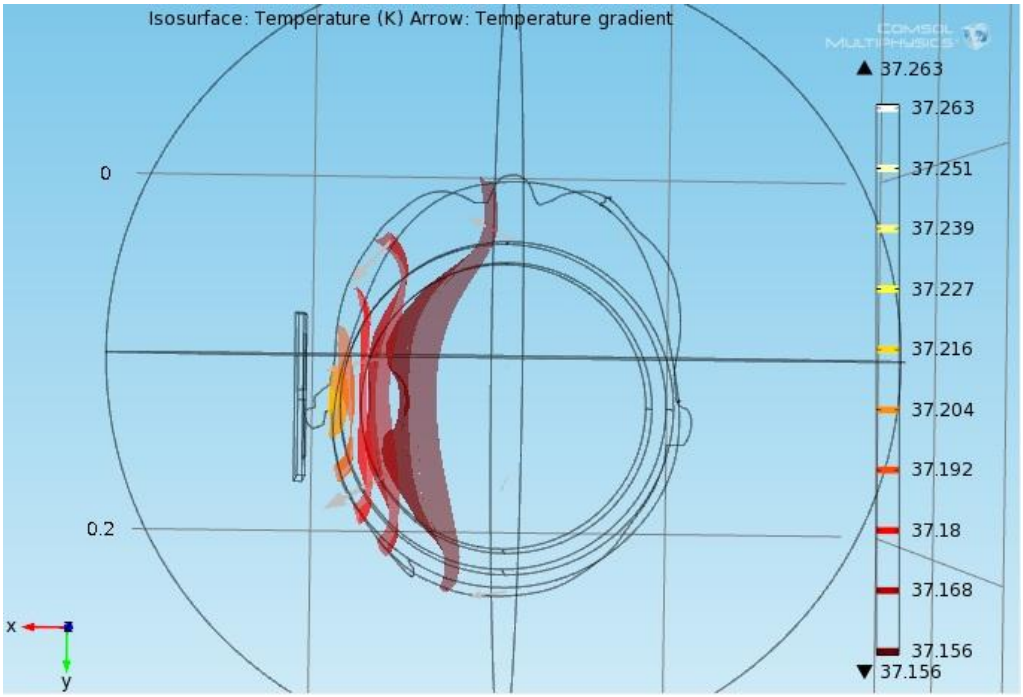


Figure 32. The contour temperature lines at 900 MHz and 0.25 W antenna power with convective cooling boundary conditions in nonhomogeneous model.

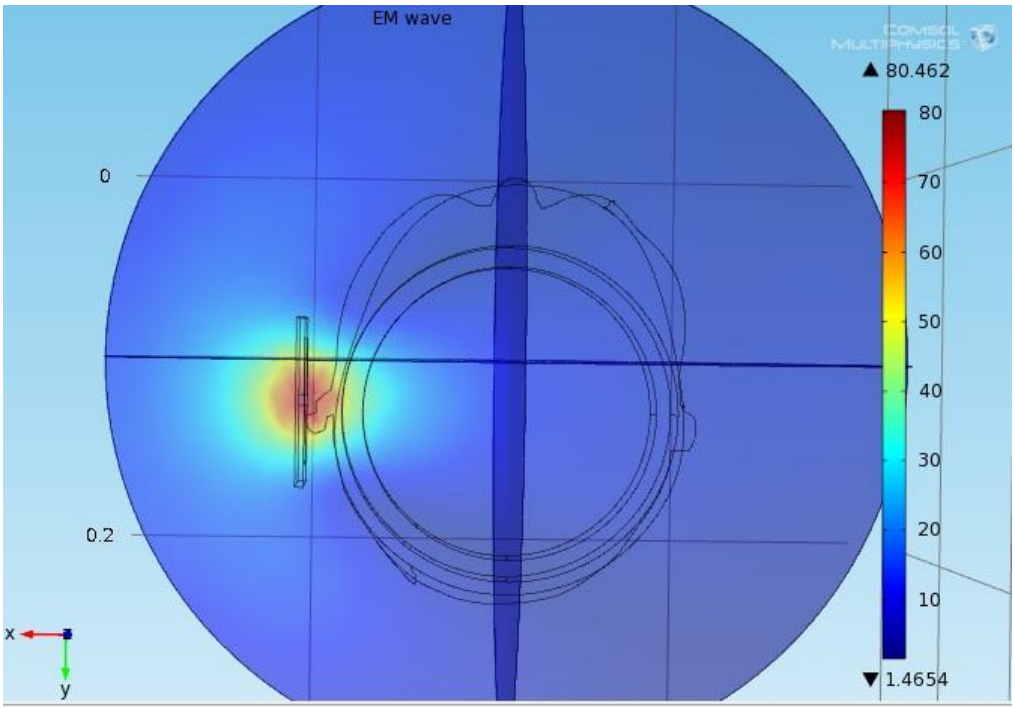


Figure 33. The EM field propagation at 1800 MHz and 0.25 W antenna power has a maximum 80.463 V/m value in nonhomogeneous model.

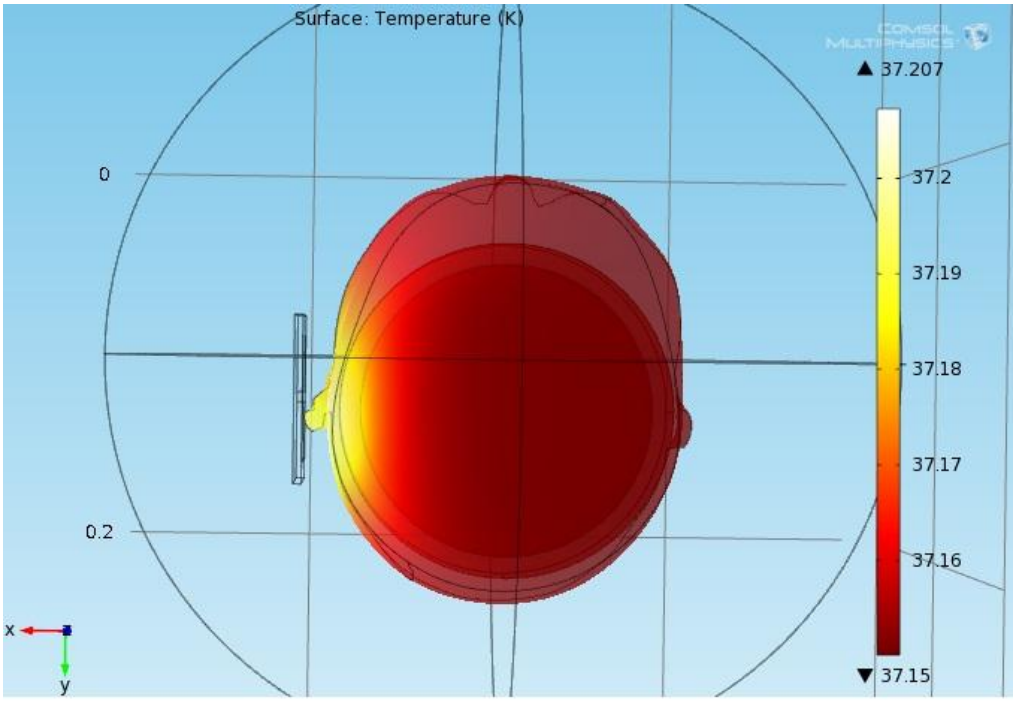


Figure 34. The local increase in surface temperature at 1800 MHz and 0.25 W antenna power with convective cooling boundary conditions has maximum 37.207 º C right beneath the antenna in nonhomogeneous model.

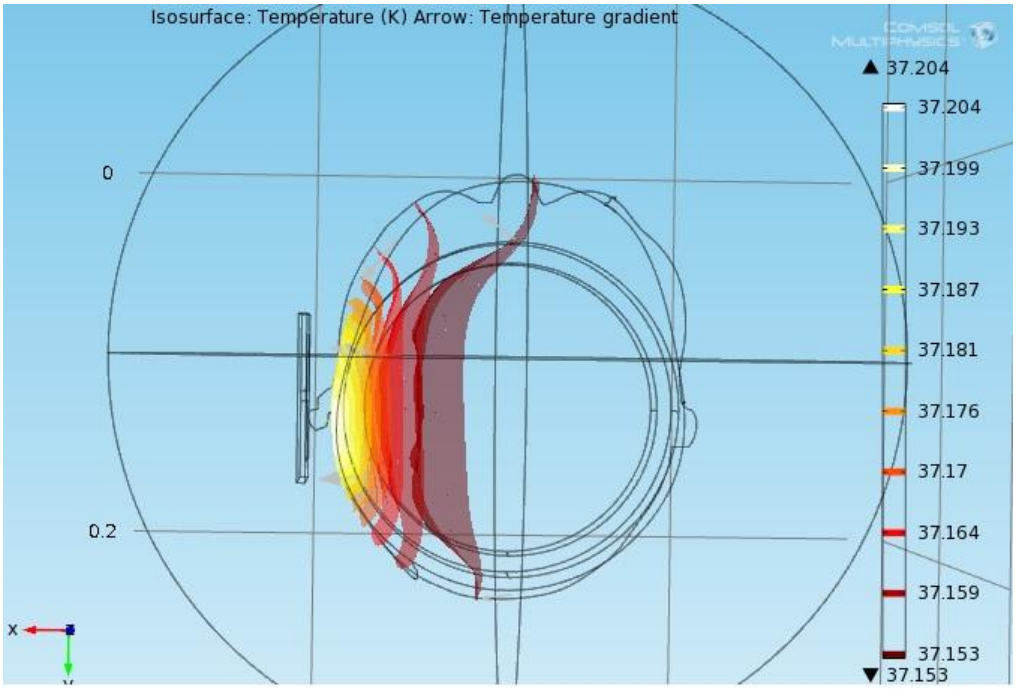


Figure 35. The contour temperature lines at 1800 MHz and 0.25 W antenna power with convective cooling boundary conditions in nonhomogeneous model.

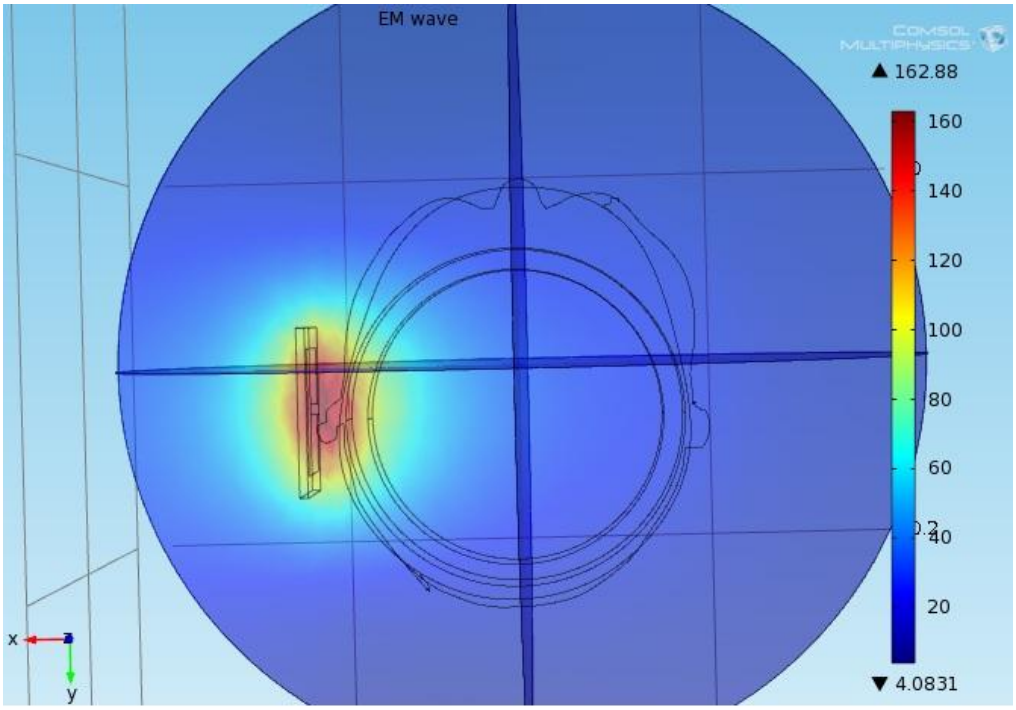


Figure 36. The EM field propagation at 900 MHz and 1 W antenna power has a maximum 162.88 V/m value in nonhomogeneous model.

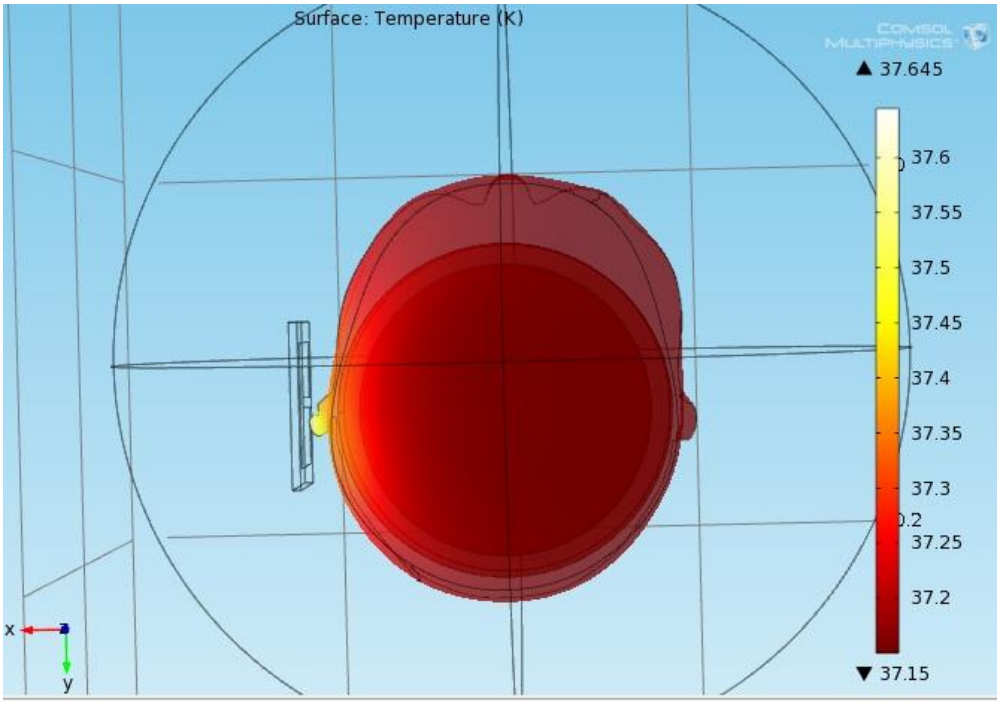


Figure 37. The local increase in surface temperature at 900 MHz and 1 W antenna power with convective cooling boundary conditions has a maximum 37.646 º C right beneath the antenna in nonhomogeneous model.

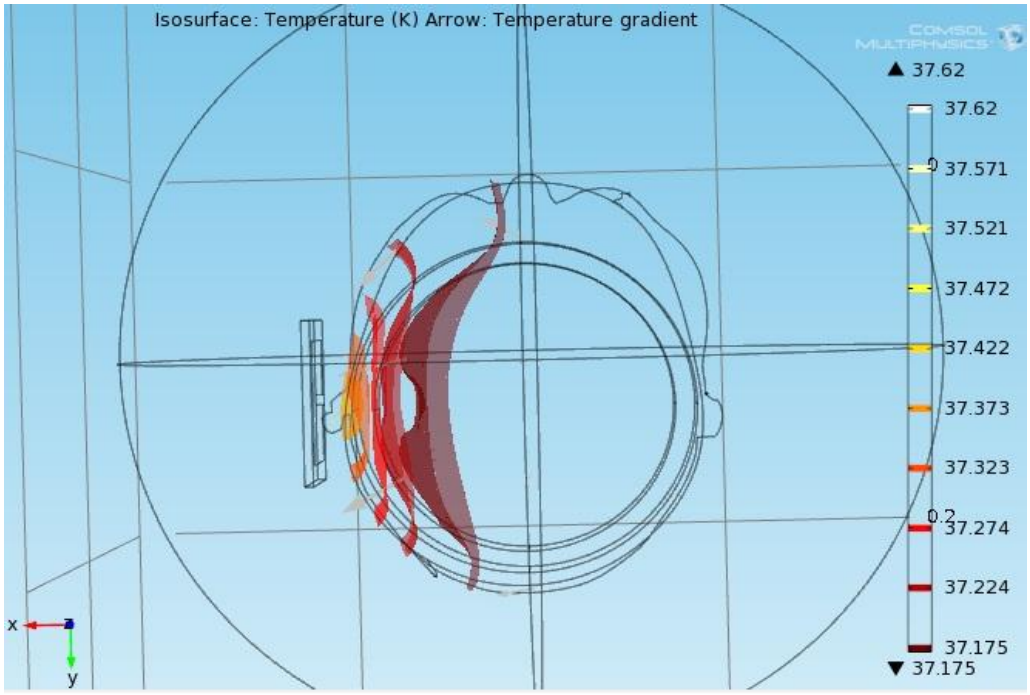


Figure 38. The contour temperature lines at 900 MHz and 1 W antenna power with convective cooling boundary conditions in nonhomogeneous model.

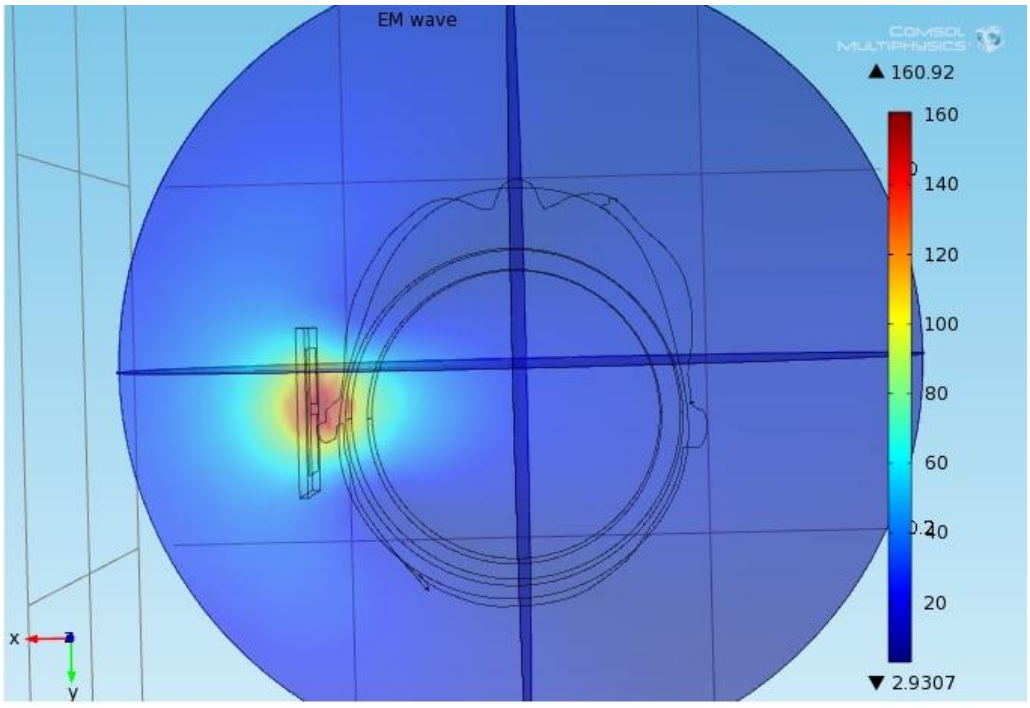


Figure 39. The EM field propagation at 1800 MHz and 1 W antenna power has a maximum 160.93 V/m value in nonhomogeneous model.

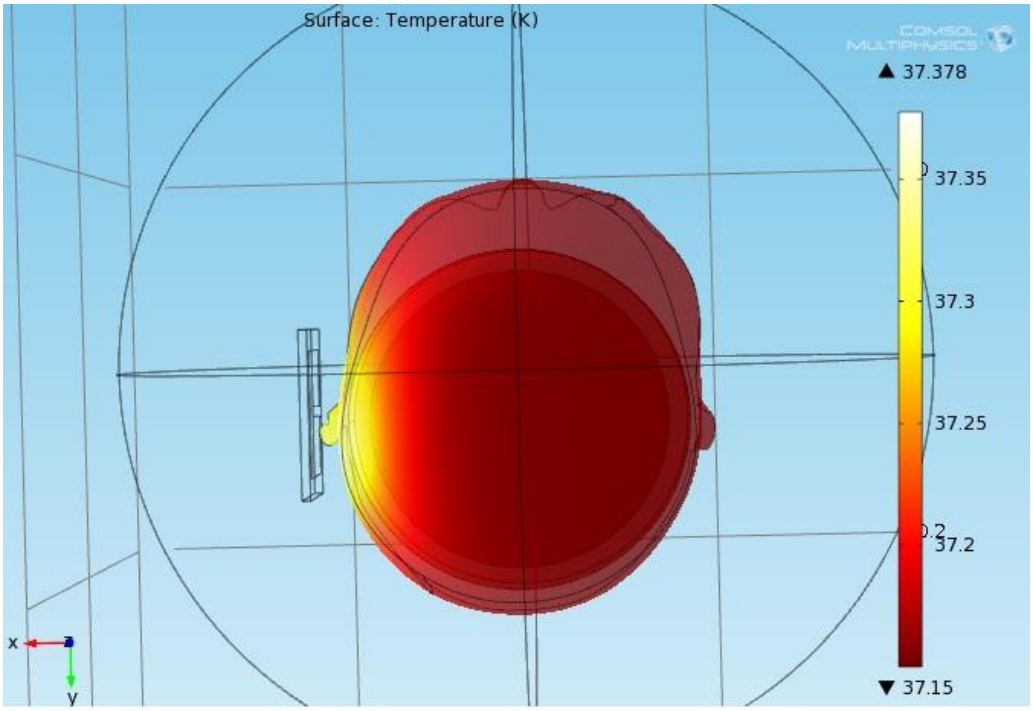


Figure 40. The local increase in surface temperature at 1800 MHz and 1 W antenna power with convective cooling boundary conditions has a maximum 37.378 º C right beneath the antenna in nonhomogeneous model.

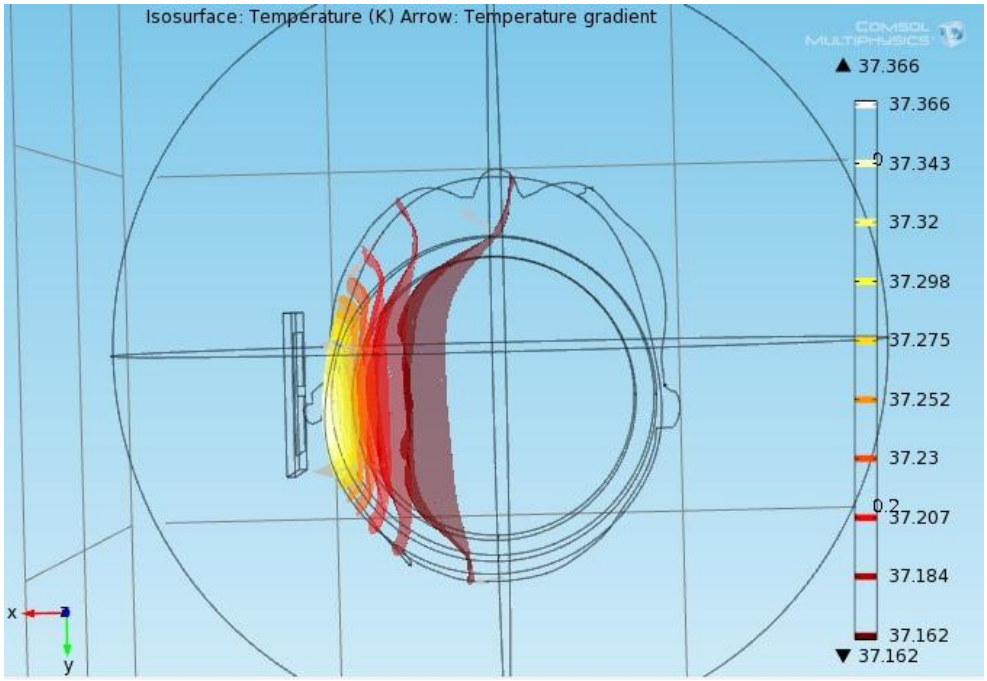


Figure 41. The contour temperature lines at 1800 MHz and 1 W antenna power with convective cooling boundary conditions in nonhomogeneous model.

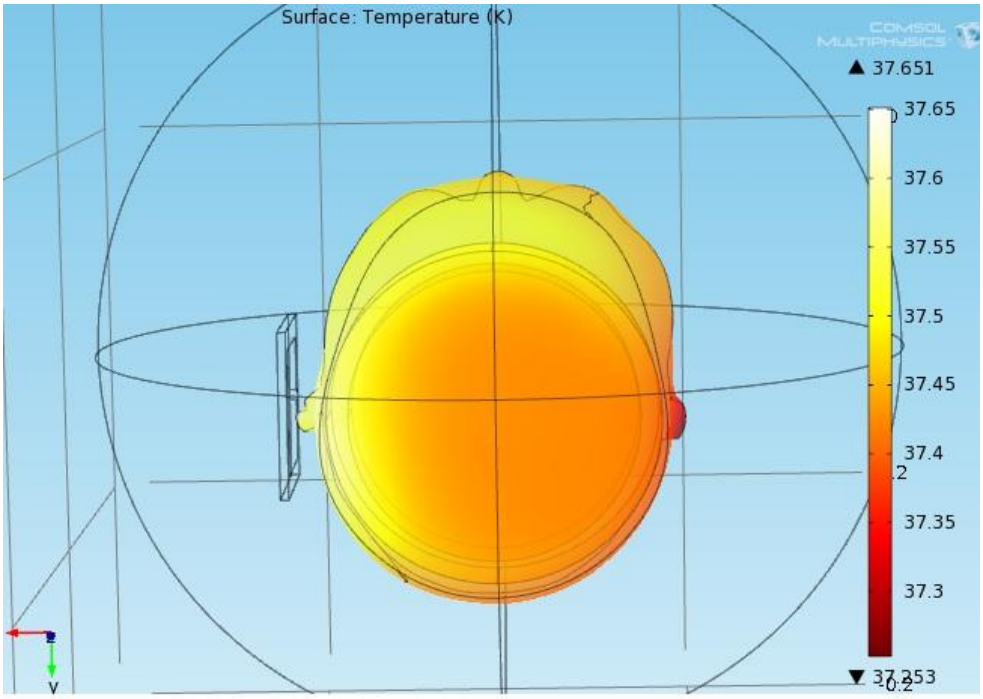


Figure 42. The local increase in surface temperature at 900 MHz and 1 W antenna power with metabolic heat source and convective cooling boundary conditions has a maximum 37.652 º C right beneath the antenna in nonhomogeneous model.

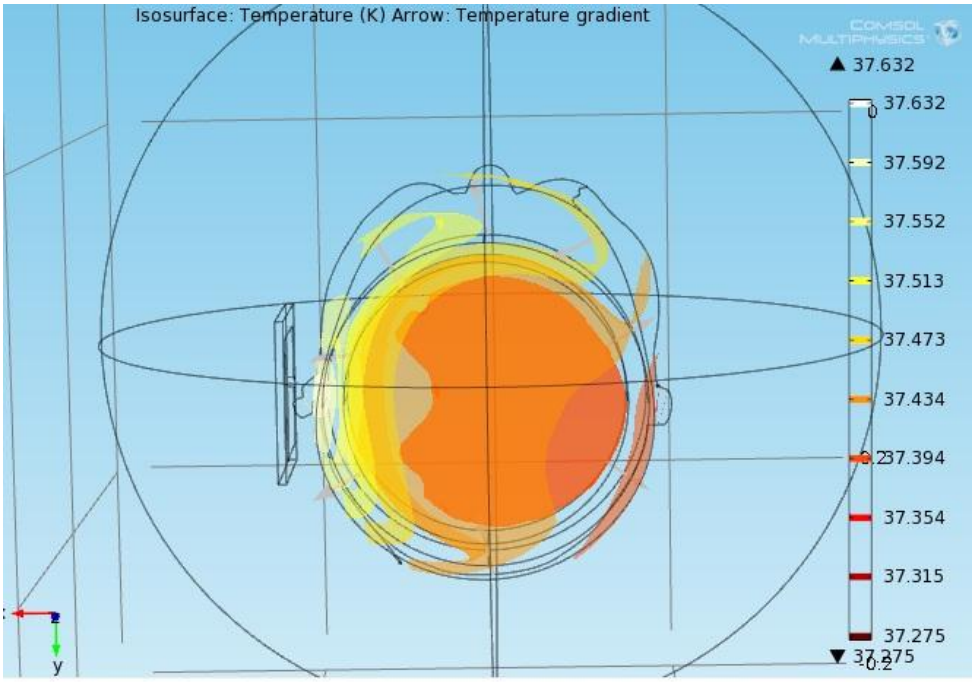


Figure 43. The isothermal contour temperature lines at 900 MHz and 1 W antenna power with metabolic heat source and convective cooling boundary conditions in nonhomogeneous model.

6. DISCUSSION AND CONCLUSION

The purpose of this study is to quantify the electromagnetic absorption and the related temperature increase in the human head due to mobile phone usage using a numerical model. We have analyzed several different cases with varying frequency, power and homogeneity of the material. We have also checked how the results are affected by the existence of a metabolic heat source and applying two different boundary conditions for the heat transfer problem. The numerical results of the analyses for both homogeneous and nonhomogeneous cases are summarized on Table 5.7.

Table 5.7. The calculated the electrical field, maximum SAR and maximum temperature rise for homogeneous and nonhomogeneous head models.

	Frequency (MHz)	Power (W)	E (V/m) max.	SAR (W/kg) max.	Temperature max.	Notes
Homogeneous model	900	0.25	55.05	0.711	37.487	Thermal insulation b.c.
	1800	0.25	57.23	0.906	Not calculated	Thermal insulation b.c.
	Frequency (MHz)	**Power (W)**	**E (V/m) max.**	**SAR (W/kg) max.**	**Temperature max.**	**Notes**
Nonhomogeneous model	900	0.25	81.440	1.59	37.270	Convective cooling b.c.
	900	0.25	81.440	1.59	37.276	Thermal insulation b.c.
	1800	0.25	80.462	0.94	37.207	Convective cooling b.c.
	900	1	162.88	6.36	37.645	Convective cooling b.c.
	1800	1	160.93	3.79	37.378	Convective cooling b.c.
	900	1	162.88	6.36	37.651	Metabolic heat source, Convective cooling b.c.

The main determinant of the SAR value is the power of the patch antenna. Under the same frequency, the SAR value is almost exactly proportional to the square of the power (Eq. 2.45). The SAR value also constitutes a heat generation in the heat transfer problem (Eq. 2.46). Hence, the temperature increase also changes almost proportionally to the power square. The proportionality is slightly perturbed because convection and conduction removes a higher amount of heat energy with

increasing temperature gradient between the tissue and the surrounding tissues and the air.

Frequency is an important factor affecting the SAR value. The electromagnetic properties of the tissues are highly frequency-dependent (Table 5.1., 5.2., 5.3. and 5.4.). As a result, under the same power, the observed temperature increase changes from one frequency to the other.

As expected, the maximum SAR increase is observed on the outer boundary of the skin-fat tissue next to the antenna. The maximum temperature increase is also observed at a spot close to the antenna. Due to convective cooling, this maximum occurs typically not on the boundary but slightly inside of the boundary. The depth at which an observable SAR is encountered depends largely on the frequency and the material properties at that frequency. It is well known that waves of lower frequency penetrate deeper into a homogeneous medium. However, in a nonhomogeneous medium with several different layers the situation is complicated by the presence of the reflection at the layer interfaces. Accordingly, the electric field penetrates deeper into the tissue at 900 MHz compared to 1800 MHz. (Figs. 24 and 27). In the nonhomogeneous model, the maximum electric field is higher for the 900 MHz case at 0.25 and 1 W (Figs 28, 36 and Table 5.8.). In agreement with that, the maximum temperature rise is also found to be higher at 900 MHz (0.495 C^o above the baseline) compared to 1800 MHz (0.263 C^o above the baseline) at 1 W (Figs 37, 40 and Table 5.7.). At 1 W, the temperature rise at the outer surface of the brain is at 0.08 and 0.07 at 900 MHz and 1800 MHz, respectively.

The effect of the metabolic heat source is, as expected, a general increase in the temperature rise in the entire head. At 900 MHz and 1 W, the maximum temperature rise is found to be 0.501 C^o, slightly above the value (0.495 C^o) observed without a metabolic heat source present (Figs 37, 42 and Table 5.7.).

We have observed that the homogeneous and nonhomogeneous models can produce different predictions in the SAR value and the temperature rise. Taking an average value of the material properties in a homogeneous model does not have the exact same effect as using a nonhomogeneous model. We can conclude that a

nonhomogeneous model makes a difference over the homogeneous model and seems to be more realistic.

Table 5.8 A comparison with nonhomogeneous FEM and FDTD head models.

Models performed at 900 MHz, 1 W.	**Temperature rise** C^o
Present study (Nonhomogeneous model)	0.495
Samaras et al, 2003. (Japanese model)	0.515
Difference	0.030

In a similar FEM study, Cazacu et al (Cazacu et al, 2009) utilized a simplistic geometry of the human head, a different set of material properties and the same frequency values in comparison to the current work. They observed a similar dependency of the SAR values to the frequency. On the other hand, their SAR values, numerically, are different than what is reported in this work. The difference seems to originate mostly from the difference in material parameter values.

Another similar study performed using FDTD method (Samaras T et al, 2003) produced a maximum temperature increase of 0.495 C^o at 900 MHz and 1 W which is comparable to our corresponding value of 0.515 C^o (Table 5.8.). The calculated maximum temperature rise in that study also occurred on the skin surface.

The objective of this study was to perform an FEM simulation of the electromagnetic absorption and the resulting temperature increase in the human head due to mobile phone usage. The results of our study give predictions about the temperature rise in the head tissues. It is the responsibility of other researchers to interpret the outcome of this study (and of other studies like) to make solid claims (if possible at all) about the potential health hazard of cell phone usage. However, we still can underline a few points:

§ The standard for maximum allowable value of SAR in Europe, as prescribed by ICNIRP and WHO (http://www.icnirp.de/), is 2W/kg. In our simulation, we have observed that the maximum SAR value can be as high as 6,36 W/kg in certain tissues in the human head for cell phone power of 1 W which is above the allowable maximum value.

- Experimental studies indicate certain physiological changes in the exposed tissues (F. Ozguner et al, 2004). This can be due to exposed radiation or due to the resulting temperature increase or both.
- Our simulation showed that the resulting temperature rise is typically small in all tissues. However, it is an open question whether long term exposure to this small rise should cause any health concerns.

REFERENCES

MUR, G., 1985. A finite element method for computing three dimensional Electromagnetic fields in inhomogeneous media, IEEE Trans. Magnet., 21, 6 : 2188 – 2191.

CINGOSKI, V., MIYAMOTO, N., YAMASHITA, 1998. H. Element – free Galerkin method for electromagnetic field computations, IEEE Trans. Magnet. 34, 5 : 3236–3239.

YUAN, X., 1990. Three dimensional electromagnetic scattering from inhomogeneous objects by the hybrid moment and finite element method, Microwave Theory and Tecn., IEEE, Trans Anten and Propagat., 38, 8 : 1053 – 1059.

CIRIC, R. I., and COORAY, F. R., 2000. Light scattering by nonspherical particles, edited by Mishehenko, M. I., Hovenier, J. W. and Travis L. D., Acad Press, NY.

YEE, K. S., 1966. Numerical solution of initial boundary value problems involving Maxwell's equations in isotropic media, IEEE Trans. Anten. Propagat., 14 : 585–589.

TAFLOVE, A., and BRODVVIN, M. E., 1975. Computation of electromagnetic fields and induced temperatures within a model of the microwave irradiated human eye, IEEE Trans. Microwave Theory Tech., 23 : 888–896.

SULLIVAN, D. M., GANDHI, O. P., 1998. Use of the Finite Difference Time Domain Method for calculating EM absorption in man models, IEEE Trans. on Biomed. Engin., 35, 3 : 179 – 186.

RIU, P. J., and FOSTER K. R., 1999. Heating of tissue by near field exposure to a dipole: a model analysis., IEEE Trans. on Biomed. Engin., 46, 8 : 911 – 917.

SINHA, B. P., and MACPHIE, R. H., 1977. Electromagnetic scattering by prolate spheroids for plane waves with arbitrary polarization and angle of incidents, Radio Sci., 12 : 171 – 184.

DALMAS, J., and DELEUIL, R., 1985. Multiple scattering of electromagnetic waves

from two infinitely conducting prolate spheroids which are centered in a plane perpendicular to their axes of revolution , Radio Sci., 20 : 575 –581.

CIRIC R. I., and COORAY F. R., 1991. Scattering by systems of spheroids in arbitrary configurations, Comput. Physc. Commun., 68 : 279 – 305.

NAG, S., and SINHA, B. P., 1996. Electromagnetic Plane wave scattering by a system of two uniformly lossy dielectric prolate spheroids in arbitrary orientation, IEEE Trans. Microwave Theory Tech., 44 : 1855 – 1864.

PENAFIEL, L, M., LITOVITZ T, KRAUSE, D, DESTA, A, and MULLINS, J. M., 1997. Role of modulation on the effect of microwaves on ornithine decarboxylase activity in L929 Cells, Bioelectromagnetics, 18 : 32.

LAI, H. and SINGH N. P., 2004. Magnetic field induced DNA strand breaks in brain cells of the rat, Environm. Health Persp., 112 : 687.

SARKAR, S., S. ALI, and BEHARI, J., 1984. Effect of low power microwave on the mouse genome: A direct DNA analysis Mutat Res., 320: 141.

STRONATI, L, A., TESTA, J., MOQUET, A., EDWARDS, E., CORDELLI, P., VILLANI, C., MARINO, A, M., FRESEGNA, M., APPOLONI and LLOYD D., 2006. 935 MHz cellular phone radiation. An in vitro study of genotoxicity in human lymphocytes, Int J Radiat Biol., 82 : 39.

NITTBY, H., BRUN, A., EBERHARDT, J., MALMGREN, L., PERSSON, B. R. and SALFORD L. G., 2009. Increased blood brain barrier permeability in mammalian brain 7 days after exposure to the radiation from a GSM – 900 mobile phone, Pathophysiology, 599.

WESSAPAN, T., SRISAWATDHISUKUL, S., RATTANADECHO, P., 2011. Numerical analysis of specific absorption rate and heat transfer in the human body exposed to leakage electromagnetic field at 915 MHz and 2450 MHz, ASME J. Heat Transfer, 133.

WESSAPAN, T., SRISAWATDHISUKUL, S., RATTANADECHO, P., 2011. The effects of dielectric shield on specific absorption rate and heat transfer in the human body exposed to leakage microwave energy, Int. Commun. Heat Mass Transfer, 38, 2 : 255–262.

WESSAPAN, T., SRISAWATDHISUKUL, S., RATTANADECHO, P., 2012.

Specific absorption rate and temperature distributions in human head subjected to mobile phone radiation at different frequencies, Inter. J. of Heat and Mass Trans., 55 : 347–359.

COURANT, R. L., 1943. Variational methods for the solution of problems of equilibrium and vibration, Bull. of the Amer. Math. Soc., 5 : 1–23.

COCCIOLIL, R., ITOH, T., PELOSIL, G., SILVESTER, P. P., 1996. Finite Element Methods in microwaves: A selected bibliography, IEEE Antennas and Propagation Magazine, 38, 6 : 34 – 48.

SEKER, S. S., OZSOY, B., MORGUL, D. A., 2002. SAR Assessment in a Human Head Model Exposed to Radiation from Mobile Phone Using FEM, IEEE International Symposium on, 2 : 662 – 666.

SULLIVAN, D. M., 2000. One-Dimensional Simulation with the FDTD Method. In Electromagnetic Simulation Using The FDTD Method; IEEE Press Series, pp. 1.

MONEDA, A. P., IOANNIDOU, M..P., CHRISSOULIDIS, D. P., 2003. "Radio Wave Exposure of the Human Head: Analytical Study Based on a Versatile Eccentric Spheres Model Including a Brain Core and a Pair of Eyeballs", IEEE, Trans. Biomed. Eng., 50 : 667- 676.

TAK, C., CHOI, M., 1996. "Adaptive Finite Element Analysis of Unbounded Electromagnetic Wave Problems" , McGill University, 29-35.

POLYCARPOU, A., C., 2006. "Introduction to the Finite Element Method in Electromagnetics", Morgan & Claypool Publishers, USA.

GEDNEY, STEPHAN, D., and UMESH, N., 1995. An Unconditionally Stable Finite Element Time-Domain Solution of the Vector Wave Equation, IEEE Microwave and Guided Wave Letters, 5, 10 : 332 – 334.

SCHMID, G., NEUBAUER, G., MAZAL, P. R., and ALESCH, F., Dielectric properties of brain tissue: measurements on humans, http://www.cost281.org/download.php?fid=531.

LEVOY, M., MRI data originally from Univ. of North Carolina (downloaded from the Stanford volume data archive at http://graphics.stanford.edu/data/voldata/).

KOVETZ, 1990. The Principles of Electromagnetic Theory, Cambridge University Press.

MOREGA, M., MOREGA, A, M., 2011. Computed SAR in human head for the assessment of exposure from different phone device antennas, Environ. Engin. and Manage. Journal, 10, 4 : 527- 533.

DE, SANTIS, FELIZIANI, V., MARADEI F, M., and BUCELLA, C., 2009. Finite Element Analysis of Temperature Increase in Vascularized Biological Tissues Exposed to RF Sources, IEEE Trans. Magnet., 45, 3 : 1682 – 1685.

BEHARI, J., 2010. Biological Responses Mobile Phone Frequency Exposure, Indian Journal of Exper. Biology, 38 : 959 – 981.

SALFORD, L. G., BRUN, A, E., EBERHARD, J. E., MALMGREN L, and PERSSON B, R, R., 2003. Nerve Cell Damage in Mammalian Brain after Exposure to Microwaves from GSM Mobile Phones, Environ. Health Perspectives, 117, 7 : 881–883.

FRITZE, K., SOMMER, C., SCHMITZ, B., MIES, G., HOSSMANN, K. A., KIESSLING, M., WIESSNER., C., 1997. Effect of Global System for Mobile Communication (GSM) Microwave Exposure On Blood-Brain Barrier Permeability In Rat, 94 : 465–470.

HIRATA, A., FUJIWARA, O., SHIOZAWA, T., 2006. Correlation between peak spatial average SAR and temperature increase due to antennas attached to human trunk, IEEE Trans. Biomed. Eng., 53, 8 : 1658–1664.

OZGUNER, F., AYDIN, G., MOLLAOĞLU, H., GOKALP, O ., KOYU, A., and CESUR, G., 2004. Prevention of Mobile Phone Induced Skin Tissue Changes By Melatonin In Rat: An Experimental Study, Toxicology and Industrial Health 20 : 133-139.

E. KNOT, F. SHAEFFER, J. F. TULEY, 1985, "Radar Cross Section", Norwood, MA, Artech House.

R. T. LING, 1987. Application of computational fluid dynamics CFD) methods to numerical stu electromagnetic wave scattering phenomena, 25 : 560 – 566.

GUY, A.W., 1986. Specific Absorption Rates of Energy in Man Models Exposed to

Cellular UHF Mobile-Antennas Fields, IEEE Transactions on Microwave Theory and Techniques, 34: 671-680

FELIZIANI, M., and MARADEI, F., 2000. FEM Solution of Time Harmonic Electromagnetic Fields by an Equivalent Electrical Network, IEEE Transactions on Magnetics,36, 4 : 938-941.

YANG, W.J., 1989. Biothermal fluid sciences principles and applications.

ABRAMOWITZ, M., and STEGUN I., 1964. Handbook of Mathematical functions with Formulas, Graphs and Mathematical Tables, National Bureau of Standards,Washington, D.C.

CAZACU, D., POPA, I., and IORDACHE, M., 2009. Finite Element Numerical Experiments on the Absorption of the EMF Radiation in 3D Human Head Models, 32nd International Spring Seminer on Electronics Technology, 1 – 4.

CURRICULUM VITAE

Tansu DOGAN was born on 1988, city of K.Maraş, Turkey. He completed the high school education in Adana. He graduated from the University of Sutçü İmam in Electrical and Electronical Engineering at 2009. After graduation he has started the MSc degree in the department of Electrical and Electronics Engineering in Çukurova University, since 2009. Between mounths March 2011 to October 2011, he worked at Huawei Telecom Co. for Turk Telekom's technical support department as a regional engineering supervisor in Ankara, Turkey. His team was finished the European's greatest Backbone DWDM project and awarded by the Turk Telekom. Between mounths October 2011 to March 2012, he worked at Huawei for Turkcell's technical team in İstanbul, Turkey.

His areas of interest includes FEM analysis of electromagnetic propagation, radio propagation of electromagnetic waves, NG DWDM ASON project migration, creation service and optimization, OPA and ASON function enabling for Turkcell and Turk Telekom Network, NG DWDM 40 G coherence future acceptance testing, SDH and DWDM commissioning site acceptance testing, cell planning for wireless communications.

He is a member of Turkish Chamber of Electrical Engineers.